UCID- 20502



# EVALUATION OF TEARING ENERGIES IN STYRENE-BUTADIENE RUBBERS

Alfred Goldberg
Donald R. Lesuer
Jack C. Stone
Lawrence Livermore National Laboratory
Livermore, CA.
and
Jacob Patt
U. S. Army Tank-Automotive Command
Warren, MI.

June 25, 1985

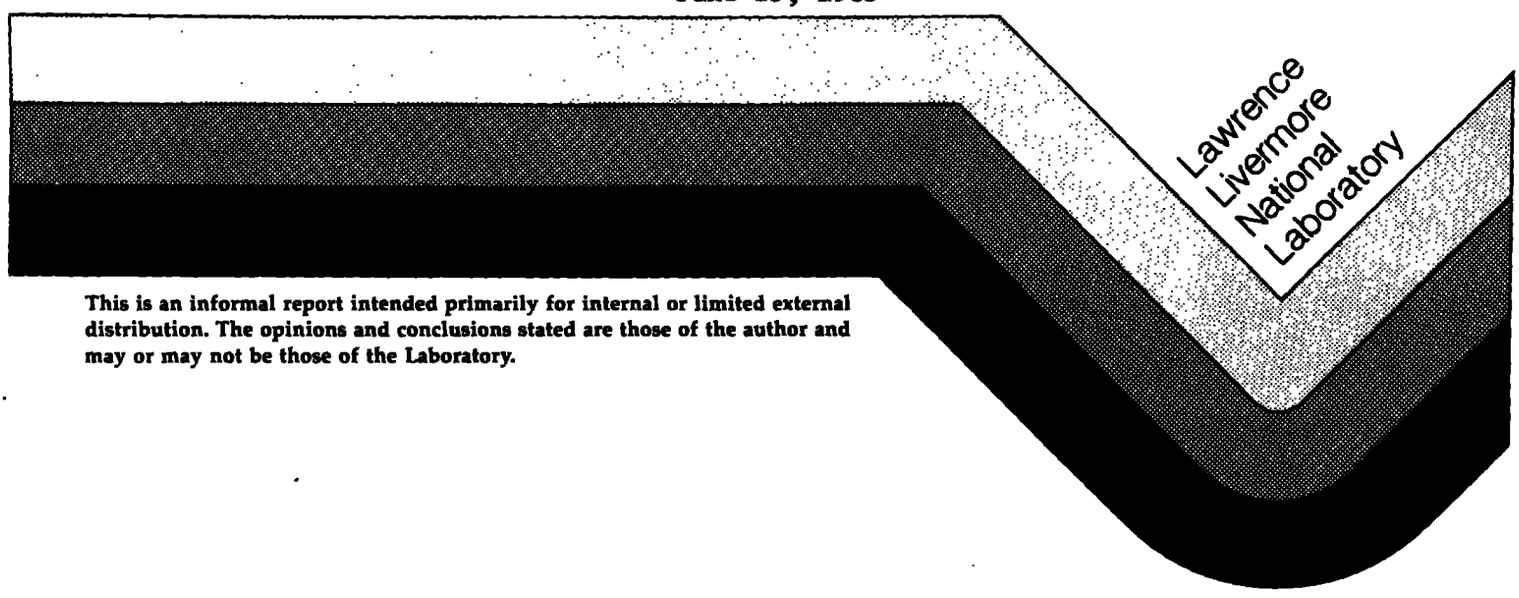

## DISCLAIMER



Printed in the United States of America
Available from
National Technical Information Service
U.S. Department of Commerce
5285 Port Royal Road
Springfield, VA 22161
Price: Printed Copy $ ; Microfiche $4.50

| Page Range | Domestic Price | Page Range | Domestic Price |
|---|---|---|---|
| 001-025 | $ 7.00 | 326-350 | $ 26.50 |
| 026-050 | 8.50 | 351-375 | 28.00 |
| 051-075 | 10.00 | 376-400 | 29.50 |
| 076-100 | 11.50 | 401-426 | 31.00 |
| 101-125 | 13.00 | 427-450 | 32.50 |
| 126-150 | 14.50 | 451-475 | 34.00 |
| 151-175 | 16.00 | 476-500 | 35.50 |
| 176-200 | 17.50 | 501-525 | 37.00 |
| 201-225 | 19.00 | 526-550 | 38.50 |
| 226-250 | 20.50 | 551-575 | 40.00 |
| 251-275 | 22.00 | 576-600 | 41.50 |
| 276-300 | 23.50 | 601-up[1] | |
| 301-325 | 25.00 | | |

[1]Add 1.50 for each additional 25 page increment, or portion thereof from 601 pages up.

# EVALUATION OF TEARING ENERGIES IN STYRENE-BUTADIENE RUBBERS*

**Alfred Goldberg**
**Donald R. Lesuer**
**Jack C. Stone**

University of California, Lawrence Livermore National Laboratory
Livermore, California 94550

**Jacob Patt**

U. S. Army Tank-Automotive Command
Warren, Michigan 48090

## ABSTRACT

Tearing energies were obtained on samples removed from commercial tank-track pads and on a series of SBR laboratory formulations in which the carbon-black content varied from 0 to 40 wt.%. The commercial materials were tested at a strain rate of $10^{-1}$/s with temperatures ranging from 22 to 140° C. The laboratory materials were tested also at both lower and higher strain rates and at -20° C. We evaluated the effect of temperature, strain rate, and carbon-black content on tearing energy, failure stress, and failure strain. The results, including the shape of the stress-strain curves, are discussed in terms of viscoelasticity, uncoiling of the long molecular chains, carbon-black rubber interactions, and knotty tearing.

In the absence of knotty tearing and for carbon-black contents of 20 wt.% or less the tearing energy, the failure stress, and failure elongation increased with either a decrease in temperature or an increase in carbon-black content. With the first appearance of knotty tearing, which occurred at 20 to 25 wt.% carbon black, large increases in tearing energy and failure strength were obtained. Between 25 and 40 wt.% carbon black both tearing energy and failure stress varied irregularly with either the carbon-black content or temperature. The

*Work performed for the U.S. Army Tank-Automotive Command, Warren, Michigan, under the auspices of the U.S. Department of Energy by the Lawrence Livermore National Laboratory under Contract No. W-7405-ENG-48.

trends obtained with the commercial materials are consistent with those exhibited by the laboratory formulations in the 25 to 40% carbon-black range. The results for the 35-wt.% formulation fell within the range of results obtained for the commercial materials.

## TABLE OF CONTENTS

## LIST OF TABLES

## LIST OF FIGURES

## LIST OF FIGURES (continued)

## 1. INTRODUCTION

Relative to the reliability of other tank components, the performance of tank track pads over most types of terrains is far from acceptable. The frequent premature wear, fracturing, and chunking of these pads result in costs amounting to several hundred million dollars annually. As part of an overall program supported by the U.S. Army, we have been involved in evaluating mechanical properties and deformation behavior of a number of styrene-butadiene polymeric elastomers, which are loaded with various amounts of carbon-black filler. Both laboratory-prepared formulations and samples cut out of commercial tank pads were evaluated. In this paper we report primarily on the tearing energies and failure stresses obtained for these materials tested at various temperatures and strain rates. We also include stress-strain curves for a number of the laboratory formulations and some discussion on strength and tearing behavior.

As first formulated by Rivlin and Thomas[1] the tearing energy can be described in terms of the strain-energy release rate of an advancing tear, in that the driving force for the tearing is provided by the release of stored elastic strain energy. The tearing becomes critical, i.e., self-propagating, when the decrease in this energy is equal to or greater than the work required to propagate the tear.

Various sample configurations have been used to evaluate the tearing energy, with the results virtually being independent of the type of test and/or sample configuration used.[2,3,4] The derivations all consider that the overall strain-energy release rate is closely related to the strain-energy density at the tear tip. In our studies we elected to evaluate tearing energies using double-edge-nicked flat samples.

In a previous report[5] we discussed in some detail the tearing behavior of a number of SBR formulations tested under a wide range of temperatures and strain rates. Included in that report were evaluations of torn and fractured surfaces of many of the samples listed in the present paper. Of special interest were the initiation and propagation

of tears that approached directions parallel to the tensile axis. These tear deviations have been ascribed to a strength-anisotropy phenomenon[6] that is developed in the deformation of carbon-black-loaded elastomers tested under certain conditions of temperature and strain rate. This deviated tearing is frequently referred to as "knotty tearing" because of the knot-like features seen on the torn surfaces. It has been suggested that the blunting of the tear front, resulting from this deviated tearing, causes an increase in tensile strength and tearing energy of the elastomer, adding to the strengthening effect imparted by the carbon black, per se.[2,6,7,8] In the present paper we examine the role of this phenomenon in attempting to relate our calculated tearing energies to the stress-strain curves of the un-nicked corresponding samples to the tensile strength of both nicked and un-nicked samples, and to the effect of strain rate, temperature, and carbon-black loadings.

## 2. EXPERIMENTAL

### 2.1 Test Materials

The materials evaluated are listed in Table 1. Styrene-butadiene rubber (SBR) is the polymeric component in both types of materials. The carbon-black content of the laboratory formulations ranges from 0 to 40 wt. %; the 35-wt. % content is close to that contained in commercial tank track pads. Most of the laboratory formulations were compounded and cured by Burke Industries, San Jose, CA. The materials were obtained in the form of 6 in. x 6 in. (152 mm x 152 mm) sheets, ranging in thickness from 0.070 in. to 0.095 in. (1.78 to 2.41 mm). In the later stages of the program the test materials were made in our own laboratory, providing sheets measuring 10 in. (254 mm) diameter x 0.080 in. (2.03 mm) thick. Monsanto Rheometer tests for $t_{90}$ (time to reach 90% of maximum torque) of our laboratory-compounded materials were made by Harold C. Seger, Rubber Consultant, Emeryville, CA.

Test samples of commercial materials (Goodyear, Firestone, and Standard T142 and T156 pads) were obtained from sheets that were sawed off from the actual pads. The sheets were chilled in a freon-dry ice mixture and machined to a smooth finish giving a thickness of approximately 0.100 in. (2.54 mm), the sheets being re-chilled between successive cuts. The individual sheets from a pad are identified sequentially from the surface into the interior, by the designations, A, B, C, etc.

Test samples measuring 6 in. (152 mm) long x 1.000 in. (25.4 mm) wide were extracted from the rubber sheets using a die punch. Edge nicks, approximately 0.050 in. (1.27 mm) deep, were introduced using a sharp razor blade. Fractography of samples tested early in this study revealed uneven cut tips. This problem was eliminated with an adjustable centering jig clamped on to the sample while it was being nicked.

## 2.2 Test Procedure

Samples were tested on an Instron universal testing machine at temperatures ranging from -20 to + 140° C (-4 to + 284° F) using a temperature-controlled chamber that could either be heated or cooled by air circulating through a refrigeration/heating unit. Initially, screw-clamped grips were used with a distance of about 3.5 in. (88.9 mm) between grips. A standard crosshead speed of 0.33 in./s (8.33 mm/s) was used giving a load-displacement strip-chart record. Conversion to strain was based on calibration runs using 1-in. (25.4-mm) gage marks. Later in the program the clamp grips were replaced with Instron elastomeric grips. We also began using an Instron 1-in. gage-length incremental extensometer having 0.10-in. (2.54-mm) increments extending over a 10-in. (254-mm) range. The 0.10-in. extension increments are ticked off on the load-displacement strip-chart record.

In addition to testing at the standard speed, some of the laboratory formulations were tested at stroke-displacement rates of about 235 in./s ($6 \times 10^3$ mm/s) and $6.6 \times 10^{-4}$ in./s ($1.68 \times 10^{-2}$ mm/s).

The high stroke rate was obtained on an MTS machine having an open-loop stroke* capability of up to 235 in./s (with a closed-loop stroke capability of up to 15 in./s). The output data of load and extension were fed to a digital transient recording system integrated with a Digital Equipment Corporation LSI-11 minicomputer for data acquisition, processing, and graphics.

A limitation of 10 in. in stroke travel in the high strain-rate system required modifications of the test samples. In addition, in order to reduce the inertia of the sample-and-grip-combination, small aluminum screw-clamped grips were used. For nicked samples, the separation between grips measured 1.63 in. (41.3 mm). Dogbone-shaped strips, with a 0.5 x 0.5 in. (12.7 x 12.7 mm) reduced gage region, were used for the un-nicked samples.

The test records were processed using an HP 9845B desk computer with an HP 9874A digitizer. The results were automatically plotted on an HP 7470A plotter yielding the final stress-strain curves. Both engineering and true stress-strain data were obtained; however, in this paper we present only the engineering values. Stresses reported for nicked samples are nominal stresses, i.e., values are based on the pre-nicked cross sections.

## 2.3 Evaluation of Tearing Energy

Following the scheme proposed by Oh[9] the tearing energy, $T_t$ is given by:

$$T_t = 2k(\lambda)cWt \text{ (for thickness t)} \qquad (1)$$

where

$k(\lambda)$ = a proportionality factor varying with the stretch ratio, $\lambda$ ,
$c$ = cut depth,
$W$ = stored strain-energy density far removed from the cut, and
$t$ = undeformed thickness.

* In the remainder of the report the term crosshead will be used for both crosshead and stroke (ram) displacements.

Dividing by t, we obtain the tearing energy T per unit thickness as:

$$T = 2k(\lambda)cW \qquad (2)$$

Using the stress value at which the nicked sample failed as the critical limiting stress on the stress-strain curve of a corresponding un-nicked sample, the value of W is then determined from the area under this curve. A minor error is introduced by considering that all the strain energy is recoverable. The hysteretic loss is assumed to be small compared to variations within a given formulation. The values of c, t, and $\lambda$ are measured for each sample. The parameter $k(\lambda)$ is determined from the curve given by Oh.[9]

## 3. RESULTS

### 3.1 Tearing-Energy Data

The tearing-energy data for the laboratory formulations and commercial materials are plotted in Tables 2 through 8 and 9 through 11, respectively. Under the heading of test numbers the first number refers to the un-nicked sample, the second number to the corresponding nicked samples. The failure stresses refer to the nicked samples. In some cases, the relative tearing energies may appear to be quite inconsistent with the corresponding stress levels. This is due to differences in the sample cut depth, c, used in equation (2). In general, considerable scatter in the data is obtained. However, several trends were detectable.

Figures 1 and 2 contain plots of the average values* of tearing energy obtained at a crosshead rate of 0.33 in./s as a function of temperature for the individual laboratory formulations and commercial

* Average values are used in all plots throughout this report.

pads, respectively. Data for the SBR-35 formulation are included in the plots of Fig. 2. It appears that at this carbon-black content a maximum in tearing energy is obtained at about 60°C. The formulations of SBR-25, -30, and -40 also show either a maximum or at least deviations from the normally expected trend of a decrease in tearing energy with an increase in temperature. The expected trend is obtained with the lower carbon-black contents of SBR-0, -15, and -20. The SBR-35 formulation also shows a maximum at 60°C for the tearing energy results obtained at the crosshead rate of 235 in./s; see Fig. 3. The variation of tearing energy with carbon-black content is shown in Figs. 4 and 5 for crosshead rates of 0.33 and 235 in./s, respectively. At the two lowest temperatures, 22 and -20° C, at the slow strain rate and at all test temperatures at the fast strain rate there is a general increase in tearing energy with an increase in carbon-black content. However, maxima in tearing-energy values are obtained over the range of 25 to 35 wt.% carbon black for samples tested at the three highest temperatures at the slow strain rate.

We obtained very limited data on the effect of strain rate on tearing energy. The results are shown plotted in Fig. 6. Except for one data-point of SBR-35 obtained at the slowest strain rate, the tearing energy increases with an increase in strain rate. An explanation of the various trends and/or anomalies observed was sought in the stress-strain behavior of the corresponding un-nicked samples, in the failure stresses, and in the extent of deviated, knotty, tearing as observed in the failed nicked samples.

### 3.2 Stress-Strain Curves At 0.33 in./s

Engineering stress-strain curves of un-nicked samples tested to failure at 0.33 in./s at various temperatures are shown in Figs. 7 through 13 for SBR-0, -15, -20, -25, -30, -35, and -40, respectively. Except in a few cases, e.g., for SBR-0, only one curve for each test condition is shown. Note that the insert in Fig. 7 for SBR-0 is drawn on the same scale used for all other formulations.

Except for one abnormally low stress-strain curve at 22°C, the data for SBR-0 are closely grouped together with their positions being random relative to temperature. This also follows with SBR-15. With the higher carbon-black contents, however, the curves obtained at 22° C and/or -20° C are displaced above those curves that are grouped together at the higher temperatures. For all formulations there is a general decrease in failure stress with an increase in temperature.

In Figs. 14 through 18 the stress-strain curves for the un-nicked samples are redrawn to illustrate the influence of carbon-black content at each test temperature. Four main features are illustrated. Firstly, at all temperatures the stress-strain curves are displaced to higher stress values (i.e., an increase in stiffness) with increasing carbon-black content, although some overlapping of the SBR-30 and -35 curves is seen at the three highest temperatures. Secondly, there is a maximum in elongation at about 20 to 25 wt. % carbon black with a sharp fall-off with decreasing amounts of carbon-black content. Thirdly, the failure stress increases with carbon-black content up to about 20 to 25 wt. % and thereafter the variation is random. Fourthly, the slope of the stress-strain curve (i.e., the strain hardening rate) first decreases and then increases with increasing strain. The inflection point, the strain at which a reversal in the change in strain hardening rate occurs, shifts to lower strains with an increase in carbon-black content. However, the inflection point appears to vary randomly with temperature for any given carbon-black content.

Since the only data required from nicked samples for the tearing-energy calculations are the failure stresses, the corresponding stress-strain curves were not processed from the load-displacement records. However, we have shown that for the size of nicks used in this study, the stress-strain curves of the nicked samples virtually superimpose on those obtained from corresponding un-nicked samples, although, depending on the nick depth, the failure stresses may be significantly below those of the un-nicked samples. Also, the trends reported above for the un-nicked samples are consistent with the results reported in a previous study,[5] which showed the influence of carbon black on stress-strain behavior of single-edge-nicked samples.

### 3.3 Failure-Stress Plots

Figures 19 and 20 show, respectively, the failure stress as a function of temperature for nicked and un-nicked laboratory-formulated samples. Average values are plotted where more than one sample was tested. Figure 20 shows that for the un-nicked samples the failure stress generally decreases with an increase in test temperature. However, irregular trends are obtained in Fig. 19 for nicked samples that contain more than 20% carbon black. The failure stresses are re-plotted in Figs. 21 and 22 as a function of carbon-black content for the nicked and un-nicked samples, respectively. When plotted in this manner both nicked and un-nicked samples exhibit the same general pattern, namely, a continuous increase in failure stress up to about 25 wt % carbon black followed by one or more maxima. However, exact correspondence in these maxima for a given carbon-black content is not obtained on comparing both sets of plots.

Figures 23 and 24 contain plots of failure stress as a function of strain rate of SBR-0, -15, and -35 for nicked and un-nicked samples, respectively. As may be expected a predominant trend of an increase in failure stress with an increase in strain rate is obtained. However, several deviations from this trend can be noted, especially for SBR-35, which in part could be attributed to the knotty-tearing behavior described below. In addition, some of the samples tested at high strain rates could not be taken to failure due to the test-machine limitations.

### 3.4 Deviated, Knotty Tearing

In a previous report[5] we discussed in detail observations on deviated, knotty tearing obtained on deformation of SBR-35; the extent of such behavior increased with either a decrease in strain rate or an increase in temperature. The term "deviated tearing" referred to tearing in a direction that deviates from the normal to the tensile axis, while the term "knotty tearing", as commonly used in the literature,[2,6,7,8] refers to the knot-like tears, frequently having a

chevron-like character, resulting from the intersection of individual, discontinuous tear paths. In the extreme case, which was not uncommon, the deviation was observed to be 90°, i.e., parallel to the tensile axis. Increases in both strength and tearing energy have been attributed to an effective blunting at the tear tip as the tear deviates from the normal to the tensile loading axis.

For the present paper, we made a cursory examination of the fractured samples listed in Tables 2 through 8. We noted the extent and sharpness of the deviation when it was present. Our observations are summarized in Table 12. The degree of deviated, knotty tearing is rated from 0 to 10, with zero indicating a complete absence of this behavior and 10 a maximum. The ratings are based on the sharpness of the deviation and, to a lesser extent, on the projected length parallel to the tensile axis. We noted two basic types of such tearing. In one type, the entire deviation runs parallel or nearly parallel to the tensile axis and it is terminated with the tearing direction changing abruptly to a direction normal to the tensile axis, becoming unstable and leading to failure. With our samples the extent of this deviation ranges from 0 to a maximum of 3.8 mm projected tear length. Also, the deviated tearing here has markings characteristic of knotty tearing, which can be seen with the naked eye. In the second type, the initiation, progress, and termination of the deviated tearing are all relatively gradual, with the maximum disorientation along a deviation ranging from about 15° to almost 75° from the normal to the tensile axis, with the maximum projected tear length being 5.5 mm. At low magnification (<10x) no markings were observed along these deviated tears. Examples of both types of deviated tearing were illustrated in a previous report.[5] In Table 12 we list the first type under "sharp" and the second type under "gradual." In some cases a rating is listed under both headings indicating a transition from the first to the second type of behavior. However, in these latter samples, the characteristic knotty tearing markings are either relatively weak or entirely absent. With few exceptions, deviated tearing was limited to the four highest

carbon-black loadings and at the standard and slower strain rates. Some slight indication of deviated tearing is present in SBR-20 samples tested at 140° C and in SBR-35 samples tested at the fast strain rate at 60 to 140° C. In general, the deviated tearing is favored by an increase in temperature and/or a decrease in strain rate; however, a number of exceptions are present. The irregularities in tearing energies and tensile strengths seen in the various plots could be related to the corresponding irregular trends observed in the deviated tearing. This possibility is examined below.

## DISCUSSION

The influence of temperature, strain rate, and carbon-black loading on the mechanical properties of SBR formulations has been reported in a number of papers.[2,7,8,10,11] In general, a decrease in temperature or an increase in strain rate leads to an increase in strength and tearing energy. The addition of carbon black results in large increases in both of these properties as well as developing peak values in the regime where knotty tearing prevails.[2,8] Our results are generally consistent with these observations.

For our formulations that did not exhibit any deviated, knotty tearing (SBR-0, -15, and -20) the tearing energy increases with either an increase in carbon-black content, a decrease in temperature, or an increase in strain rate (Figs. 1,3-6). The corresponding failure stress for both nicked and un-nicked samples follows the same pattern (Figs. 19-24). Between about 15 and 25 wt.% carbon black large increases in both tearing energy and failure stress occur with an increase in filler content. Between 25 and 40 wt.% carbon black these two properties appear to vary irregularly with the filler content (Figs. 4, 21, 22). The influence of temperature on tearing energy and failure stress for the high carbon-black contents (Figs. 1, 3, 19, 20) only partly follow the trends seen with the low carbon-black contents. There is either a leveling off or a maximum between about 20 to 60° C. The tearing

energies of the commercial pads also follow this general trend; they are generally consistent with the values obtained with the SBR-35 formulation (Fig. 2).

In comparing the engineering stress-strain curves for the different carbon-black contents of unnotched samples tested at a given temperature (Figs. 14-18) several features can be noted:

1. A maximum in failure strain is obtained at some intermediate value of carbon-black content.

2. Over the lower range of carbon black the failure stress increases with an increase in filler content; over the higher range this stress appears to vary randomly at the lower test temperatures, but increases with addition of filler content at the higher test temperatures.

3. The initial stage of deformation exhibits a continuous decrease in strain hardening rate with increasing strain; this is typical of most materials. This behavior is present along the entire curve for all the SBR-0 tests. However, for the carbon-black-loaded formulations an inflection* occurs leading to an increase in the strain hardening rate with strain, virtually until failure. The strain at which the inflection occurs appears to be independent of temperature for a given carbon-black content (Figs. 7-13), but at a constant temperature it appears at increasingly lower strains with an increase in the filler content (Figs. 14-18). There is a slight indication of an inflection point on curves obtained from several SBR-0 samples.

* Although the corresponding true stress-true strain curves are more fundamental and indicative of the instantaneous behavior than are the engineering curves, the inflections we illustrate here are not always detectable on the true curves.

Using the molecular coiled-chain model proposed by Flory,[12] we can assume that in the early stages of deformation the flow-stress will depend largely upon the relative ease in the uncoiling of the entangled long molecular chains. The flow stress developed during the latter stages of deformation, leading to eventual failure, and the corresponding tearing energy will depend largely upon the resistance to the movement of molecular segments, the breaking of bonds or aggregates of bonds, and the ability to dissipate energy and/or reduce stress concentrations in the vicinity of a tear tip as a tear propagates to final failure. Phenomenologically, the magnitude of these properties is related to the degree of the hysteretic heating developed during the deformation and reflects the viscoelastic behavior of the rubber. Over a wide range of temperatures and strain rates the ability of the long molecular chains, molecular segments and/or crosslinks to respond to the applied loadings decreases with either an increase in strain rate, a decrease in temperature, or an increase in carbon-black loading. At some low temperature (glass transition) or very high strain rate the thermal motions are restricted to the extent that the rubber loses its viscoelastic characteristics, i.e., stress and strain are in phase and the material behaves elastically. It would be expected that the addition of carbon black will facilitate achieving this condition. Similarly, either at some elevated temperature or at a sufficiently low strain rate the thermal motions are able to respond to the applied loadings with the elimination of a phase lag; the material now behaves elastically. Again, one may expect that with carbon-black additions either the temperature will be raised or the strain rate will be lowered at which this condition is achieved.

The exact role of the filler on increasing the inherent resistance of the elastomer to deformation, the initiation of flaw (crack) opening, and the propagation of a crack is still unclear. It is generally considered that a layer of polymer is absorbed onto the surface of the carbon black thereby producing a shell of immobilized elastomer.[13] This could cause a strengthening not unlike that of particle hardening in crystalline substances. The hysteresis has been attributed to the

breakdown of this structure.[13] It has also been suggested that the carbon-black particles act as nucleation sites for small tears at highly localized strain regions ahead of the crack, thereby blunting the main tear tip.[14]

The critical tearing energy necessary to initiate cut growth in a nicked sample is considered to depend primarily on the molecular structure, and more specifically on the energy necessary to break some minimum number of bonds.[1,3,8] For example, identical critical values are obtained for both NR and SBR gum vulcanizates. Additions of carbon black can significatively increase these values. Furthermore, the increase in applied energy required for the cut to propagate to some given depth is greater the larger is the hysteresis of the elastomer. This is consistent with the concept that the strengthening by the carbon black is due to some type of modification of the rubber structure that restrains the molecular movements.

One might suggest that the inflection corresponds to a change in the controlling mechanism that resists the applied deformation (strain hardening). Crystallization is certainly an important strengthening mechanism during the straining of natural rubber and this phenomenon may also play a role in SBR. Lyon[15], in a recent study involving calorimetric measurements during tensile straining, noted a significant increase in exothermic behavior starting at the inflection point. It may be that such crystallization take place in SBR.

The details of the processes and forces involved in the uncoiling of the long molecular chains are still unclear. Entropy is certainly a significant factor. One might consider that as the rubber is stretched the role of segmental movements becomes increasingly more important in resisting this stretching. The interactions introduced by the carbon black would result in a general increase in strength. However, the immobilized rubber-shell-carbon-black agglomerates should interfere significantly with the segmental movements. Thus, when the segmental displacements become important for further deformation, an increase in strain hardening rate is initiated (inflection point). The increased

strengthening associated with the larger amounts of carbon black would, in some manner, significantly increase the resistance to the "normal first-stage" uncoiling such that the applied deformation could be more readily accommodated through segmental movements. Thus, with further additions of carbon black the inflection is shifted to increasingly lower strains.

Alternatively, one can consider that the inflection point corresponds to the termination of the uncoiling stage in the rubber phase. Thus, the strain at which the inflection occurs would depend directly upon the relative amount of rubber phase present. In Fig. 25, the inflection strain is plotted versus carbon-black content. The data points represent average values (independent of test temperature); the bars show the range of values. If one considers all ingredients other than the carbon black as part of the rubber phase, then close to a linear relationship is obtained between the inflection strain and rubber contents over the range of 15 to 40 wt.% carbon black (curve A within the range of data points). However, an extrapolation of this near linear behavior to 0 wt.% carbon black ( 100% rubber phase) would intersect the strain axis at some value considerably below the strains where indications of an inflection point were detected on the SBR-0 stress-strain curves. Inflection points were detectable on several SBR-0 curves at strains ranging from about 155 to 165%. This suggests that the observed values for the inflection strain (Curve A) could be attributed partly to a decrease in the rubber phase (Curve B) and partly to filler strengthening phenomena, per se (Curve C), as the filler content is increased; Curve D refers to the lowest inflection strain that was observed for SBR-0. The concept is illustrated in Fig. 25.

The general decrease in failure strain with an increase in carbon-black content above some intermediate value ($\simeq$ 25 wt.%) may be due to dilution of the elastomeric phase by the filler. However, with the exception of the results obtained at 60° C (Fig. 16), the extent of this decrease becomes increasingly greater as the test temperature is lowered from 140 to -20° C. The viscoelastic (hysteretic) behavior should increase with a decrease in temperature over this temperature range. It

has been proposed[13] that the filler-elastomer interaction decreases with a rise in temperature due to a desorption and the resulting reduction in thickness of the immobilized shells of rubber absorbed on each filler particle. Thus, at the higher temperatures, where the reversal in failure strain is relatively small (Figs. 17 and 18), the filler-dilution effect is, in part, counteracted by this decrease in shell thickness. The decrease in both failure strain and failure stress obtained with an increase in temperature for a given formulation, tested at the standard crosshead speed of 0.33 in./s (Figs. 7-13), places these tests in the lower half of the parabolic-shaped failure envelope[8]. The failure envelope, which gives the failure stress and failure strain at any temperature or temperature-compensated strain rate for a given formulation, shows a maximum failure strain at intermediate temperature/strain-rate values; the strain decreases as the stress either increases in the low temperature/high strain-rate regime or decreases in the high temperature/low strain-rate regime. This behavior is consistent with the expected increased mobility and decreased strength of the elastomer with rising temperature. It may be that the failure strain is a maximum at some intermediate value that corresponds to a maximum in hysteretic (viscoelastic) behavior.

The strength and failure trends observed in our work are consistent with the generally accepted influence of test variables and carbon-black additions on the behavior of SBR formulations. The rapid rate of increase in tearing energy and failure stress between about 15 and 25 wt.% carbon black, especially at the higher test temperatures, coincides with the first appearance of knotty tearing (Figs. 4, 5, 21, 22; Table 12). However, the peaks and valleys along the plotted curves could not always be related to the extent of such knotty tearing. Part of the discrepancies may be due to sample variations; certainly, considerable scatter can be seen in the tabulated data, which list the results of each test sample. However, the regular trends observed for the lower carbon-black formulations give us confidence in the reliability of the data obtained with the higher carbon-black contents. Sampling variations (defects, curing, composition) within a given formulation and minor variations in the nicks may both greatly influence the magnitude

of the deviated, knotty tearing, which, in turn, affects the mechanical properties. In some cases, for a given formulation and test condition, the sample showing the highest resistance to failure exhibits the least amount of knotty tearing. For example, compare in Tables 7 and 12 the SBR-35 tests 136, 153, and 309 all at 140° C. By contrast, the SBR-35 tests 126, 127, and 307 at 60° C exhibit the expected influence of knotty tearing. It is clear from our studies and from studies reported in the literature that maximum or near maximum values of strength and tearing energy are associated with the presence of knotty tearing. However, it is unclear how these maxima are influenced by the depth and geometry of artificial nicks. Based on some cursory studies that we have made on cut depths we believe that this may be an important factor in influencing the degree of knotty tearing and the resulting tearing energy values. As pointed out earlier in this report, precautions were taken to minimize variations in cut depths.

## SUMMARY

Tearing energies were obtained on a number of commercial pad materials and on a series of SBR formulations in which the carbon-black content varied from 0 to 40 wt.%. Tests were performed using a standard crosshead rate of 0.33 in./s ($\dot{\varepsilon} \approx 10^{-1}$/s) at 22, 60, 100, and 140° C. The trends obtained with the commercial materials are generally consistent with those exhibited by the formulations having carbon-black contents ranging from 25 to 40 wt.%. The results for the 35-wt.% carbon-black content (close to the carbon-black content of the commercial pads) fall within the range of results obtained for the commercial materials.

For some of the experimental formulations, testing was extended down to -20° C and to both lower ($\approx 2 \times 10^{-4}$/s)and higher ($\approx 470$/s) strain rates. Normal expected trends that could be related to viscoelasticity and carbon-black-rubber- phase interactions were obtained over the range from 0 to 20 wt.% carbon black. Tearing energy and failure stress increased with an increase in filler content and strain rate and decreased with an increase in temperature.

Relatively large increases in tearing energy and failure stress were obtained between about 20 and 25 wt.% carbon black. These increases were greatest at the highest temperature and least at the lowest temperature. The relative increases coincided with the appearance of deviated, knotty tearing.

Between 25 and 40 wt.% carbon black both tearing energy and failure stress generally varied irregularly with either carbon-black content or temperature. Deviated, knotty tearing was exhibited over most of the test variables for these formulations. However, we could not unequivocally relate the observed variations in the data to the tearing behavior. These irregular trends are probably the result of both variations in the sampling and in the razor-blade nicks. Combined, they may cause significant perturbations in the knotty tearing. Failure stress as a function of either carbon-black content or temperature varied in a more systematic manner for the un-nicked samples than for the nicked samples. The phenomenon of deviated, knotty tearing was exhibited to a significantly smaller degree in the un-nicked samples as compared to its presence in nicked samples. In general, a drop in tearing energy and failure stress was obtained with an increase in carbon-black content from 35 to 40 wt.%, and this is attributed to excessive dilution of the rubber phase by the filler. Based on the failure stresses of both nicked and un-nicked samples and on the tearing energies, an optimum carbon-black content between 30 and 35 wt.% is indicated.

Engineering stress-strain curves for un-nicked samples of the experimental formulations are presented and discussed in considerable detail. Maximum elongations were obtained at intermediate values of carbon black. For a given filler content the elongation drops off with an increase in test temperature. All the curves show strain hardening. However, the carbon-black-loaded formulations exhibit an inflection in the change in strain hardening along the stress-strain curve. The inflection appears at increasingly lower strains with increasing carbon-black content; however, for a given carbon-black

content the inflection strain is independent of temperature. The stress- strain behavior and the corresponding trends are discussed in terms of viscoelasticity, rubber networks, carbon-black-rubber-phase interactions, and filler dilution of the rubber phase.

Based on the limited data from the commercial materials together with the data from the 35-wt.% carbon-black laboratory samples, a maximum in tearing energy is developed at about 60° C for these formulations.

## RECOMMENDATIONS FOR FURTHER STUDY

1. Examine influence of nick geometry and nick depth on tearing energy relative to sample size for various sample thicknesses. If it is a material property, the critical tearing energy should be constant.

2. Perform a statistical evaluation of the relationship between mechanical properties, (including tearing energy), and the extent and type of knotty tearing of a sufficient number of samples tested under carefully controlled, reproducible conditions.

3. Evaluate the relationship between knotty tearing, type of carbon black, and tearing energy.

4. Clarify the role of carbon black on affecting the inflection strain and strain hardening rates seen on the engineering stress-strain curve.

5. Perform simultaneous calorimetric and strain measurements to ascertain the presence of crystallization and the influence of carbon black on such crystallization in carbon-black-loaded SBR.

6. Expand the study to systematically cover the range of strain

7. Compare the tearing morphologies between commercial materials and experimental formulations and relate these observations to the corresponding tearing energies.

8. Relate tearing energies to hysteretic behavior for different formulations over a matrix of temperatures and strain rates.

9. Evaluate tearing energies of samples previously exposed to cyclic damage simulating field experience.

## ACKNOWLEDGMENTS

The authors wish to thank the U.S. Army Tank-Automotive Command Research and Development Center for supporting the work reported in this document. One of the authors, Jacob Patt, was also the engineer in charge of this study for TACOM. We also wish to thank Stephan Santor and David Hiromoto for performing a number of the tests, and especially Robert Scott for his guidance with the high strain rate tests.

## REFERENCES

1. R. S. Rivlin and A. G. Thomas, "Rupture of Rubber. I. Characteristic Energy for Tearing," J. Polymer Sci., 31, p. 291, 1953

2. A. N. Gent and C. T. R. Pulford, "Wear and Tear of Rubber," in Developments In Polymeric Fracture -1, (Ed. E. H. Andrews), Publ., Applied Science Publishers, Ltd., London, Gr. Br., p. 155, 1979.

3. G. J. Lake, "Aspects of Fatigue and Fracture of Rubber", in Progress of Rubber Technology, Publ., Applied Science Publishers, Ltd., London, Gr. Br., p. 89, 1983.

4. A. N. Gent, P. B. Lindle, and A. G. Thomas, "Cut Growth and Fatigue of Rubbers. 1. The Relationship Between Cut Growth and Fatigue," J. Appl. Polymer Sci., 8, p. 455, 1964.

5. A. Goldberg, D. R. Lesuer, J. C. Stone and J. Patt, "Tearing, Cut Growth, and Fracture of Styrene-Butadiene Rubber and Natural Rubber Containing Various Amounts of Carbon Black," UCID 20287, November 26, 1984, Lawrence Livermore National Laboratory, Livermore, CA 94550

6. A. N. Gent, "Some Aspects of the Tear Strength of Elastomers," in Elastomers: Criteria for Engineering Design," (Eds. C. Hepburn and R. W. Reynolds). Publ., Applied Science Publishers, Ltd., London, Gr., Br., p. 57, 1979.

7. H. W. Greensmith, "Rupture of Rubber. IV. Tear Properties of Vulcanizates Containing Carbon Black," J. Polymer Sci., 21, p. 175, 1956.

8. A. N. Gent, "Strength of Elastomers" in Science and Technology of Rubber, (Ed. F. R. Eirich), Publ. Academic Press, New York, N.Y., p. 419, 1978.

9. H. L. Oh, "A Simple Method for Measuring Tearing Energy of Nicked Rubber Strips," in Proceedings of the Eight National Symposium on Fracture Mechanics, 1974, ASTM STP 590, Publ. American Society for Testing and Materials, Philadelphia, PA., p. 104, 1976.

10. A. Kadir and A. G. Thomas, "The Behavior of Rubbers Over a Wide Range of Rates," in Elastomers: Criteria for Engineering Design, (Eds. C. Hepburn and R. J. W. Reynolds), Publ. Applied Science Publishers, Ltd., London, Gr. Br., p. 67, 1979.

11. H. W. Greensmith and A. G. Thomas, "Rupture of Rubber. III. Determination of Tear Properties," J. Polymer Sci., 18, p. 189, 1955.

12. P. J. Flory, Statistical Mechanics of Chain Molecules, Publ. Interscience Publishers, New York, N.Y., 1969.

13. Zvi Rigbi, "Reinforcement of Rubber by Carbon Black," Rubber Chem. Technol., 55, p. 1180, 1982.

14. A. N. Gent and C. T. R. Pulford, "Micromechanics of Fracture in Elastomers," J. Materials Sci. 19, p. 3612, 1984.

15. Richard E. Lyon, "Thermodynamics of Deformation," Ph.D. Thesis, May 1985, Polymer Science and Engineering Department, University of Massachusetts, Amherst, MA. 01002.

AG011

**TABLE 1. Designations of Elastomers Tested**

**A - Laboratory Formulations of Styrene Butadiene Rubber Samples**

| Ingredient | phr | Ingredient | phr |
|---|---|---|---|
| SBR-1500 | 100 | CBS Santocure | 1.0 |
| Sulfur | 1.75 | Octamine | 1.0 |
| Stearic Acid | 2.0 | Dutrex 726 | 6.0 |
| Zinc Oxide | 5.0 | HAF Black-N330 | Variable |

| | Carbon-Black (CB) | |
|---|---|---|
| Designation | phr | wt.% |
| SBR-0 | 0 | 0 |
| SBR-15 | 20.6 | 15 |
| SBR-20 | 29.2 | 20 |
| SBR-25 | 38.9 | 25 |
| SBR-30 | 50.0 | 30 |
| SBR-35 | 62.9 | 35 |
| SBR-40 | 77.8 | 40 |

Curing: 55 minutes at 145.5° C (294° F); based on $t_{90}$ for SBR-0 as provided by vendor, Burke Industries, San Jose, CA. Curing time of LLNL compounded materials may have been slightly modified based on $t_{90}$ obtained by Harold C. Seger, Rubber Consultant.

**B - Commercial Materials**

| Designation | Manufacturer | Track Shoe Design |
|---|---|---|
| G-T142 | Goodyear | T142 |
| G-T156 | Goodyear | T156 |
| F-T142 | Firestone | T142 |
| F-T156 | Firestone | T156 |
| S-T142 | Standard | T142 |
| S-T156 | Standard | T156 |

A number following a designation in Tables 9, 10, and 11 identifies a specific pad, e.g., G-T142-145. In some pads an identification number was not found.

TABLE 2. Tearing Energy Data for SBR-0

| Test Numbers | $T$, °C | Cross-head Rate | | Failure Stress | | Tearing Energy | |
|---|---|---|---|---|---|---|---|
| | | in./s | mm/s | psi | MPa | in.-lb/in.$^2$ | J/m$^2$, $10^3$ |
| 225-212 | 22 | 236 | $6\times10^3$ | 197 | 1358 | 24 | 4.20 |
| -213 | 22 | 236 | $6\times10^3$ | 192 | 1324 | 26 | 4.55 |
| 618-600 | 60 | 236 | $6\times10^3$ | 96 | 662 | 10.1 | 1.77 |
| -601 | 60 | 236 | $6\times10^3$ | 100 | 689 | 10.2 | 1.79 |
| -621 | 60 | 236 | $6\times10^3$ | 85 | 586 | 7.3 | 1.28 |
| -622 | 60 | 236 | $6\times10^3$ | 113 | 779 | 17.4 | 3.05 |
| 623-603 | 100 | 236 | $6\times10^3$ | 78 | 538 | 2.0 | 0.35 |
| 624-603 | 100 | 236 | $6\times10^3$ | 78 | 538 | 3.6 | 0.63 |
| 626-604 | 140 | 236 | $6\times10^3$ | 75 | 517 | 6.2 | 1.09 |
| -605 | 140 | 236 | $6\times10^3$ | 65 | 448 | 4.5 | 0.79 |
| 750-751 | 22 | 10 | 254 | 153 | 1055 | 15.6 | 2.73 |
| -752 | 22 | 10 | 254 | 141 | 972 | 11.5 | 2.01 |
| -753 | 22 | 10 | 254 | 142 | 979 | 14.2 | 2.49 |
| 119-121 | 22 | 0.33 | 8.3 | 90 | 621 | 10.2 | 1.79 |
| -122 | 22 | 0.33 | 8.3 | 86 | 593 | 9.3 | 1.63 |
| -305 | 22 | 0.33 | 8.3 | 84 | 579 | 8.8 | 1.54 |
| 223-121 | 22 | 0.33 | 8.3 | 90 | 621 | 11.2 | 1.96 |
| -122 | 22 | 0.33 | 8.3 | 86 | 593 | 9.2 | 1.61 |
| 471-473 | 22 | 0.33 | 8.3 | 105 | 724 | 9.9 | 1.73 |
| -474 | 22 | 0.33 | 8.3 | 100 | 689 | 11.8 | 2.07 |
| 299-129 | 60 | 0.33 | 8.3 | 51 | 352 | 2.8 | 0.49 |
| -130 | 60 | 0.33 | 8.3 | 63 | 434 | 6.2 | 1.09 |
| -306 | 60 | 0.33 | 8.3 | 65 | 448 | 7.3 | 1.28 |
| 293-129 | 60 | 0.33 | 8.3 | 51 | 352 | 3.0 | 0.53 |
| -130 | 60 | 0.33 | 8.3 | 63 | 434 | 5.8 | 1.02 |
| 141-138 | 100 | 0.33 | 8.3 | 33 | 228 | 1.1 | 0.19 |
| -139 | 100 | 0.33 | 8.3 | 49 | 338 | 2.6 | 0.46 |
| -140 | 100 | 0.33 | 8.3 | 43 | 296 | 1.9 | 0.33 |
| 142-143 | 140 | 0.33 | 8.3 | 41 | 283 | 1.3 | 0.23 |
| -144 | 140 | 0.33 | 8.3 | 45 | 310 | 1.5 | 0.26 |
| -145 | 140 | 0.33 | 8.3 | 37 | 255 | 1.0 | 0.18 |
| 223-221 | 22 | $6.6\times10^{-4}$ | $17\times10^{-3}$ | 60 | 414 | 11.2 | 1.96 |
| -222 | 22 | $6.6\times10^{-4}$ | $17\times10^{-3}$ | 55 | 379 | 9.2 | 1.61 |

TABLE 3. Tearing Energy Data for SBR-15

| Test Numbers | T, °C | Cross-head Rate | | Failure Stress | | Tearing Energy | |
|---|---|---|---|---|---|---|---|
| | | in./s | mm/s | psi | MPa | in.-lb/in.$^2$ | J/m$^2$, $10^3$ |
| 226-214 | 22 | 236 | $6\times10^3$ | 987 | 6805 | 338 | 59.2 |
| -215 | 22 | 236 | $6\times10^3$ | 860 | 5930 | 271 | 47.5 |
| -216 | 22 | 236 | $6\times10^3$ | 841 | 5797 | 269 | 47.1 |
| 619-607 | 60 | 236 | $6\times10^3$ | 217 | 1496 | 54 | 9.46 |
| 627-607 | 60 | 236 | $6\times10^3$ | 217 | 1496 | 47 | 8.23 |
| 628-608 | 100 | 236 | $6\times10^3$ | 160 | 1103 | 40 | 7.01 |
| -609 | 100 | 236 | $6\times10^3$ | 162 | 1117 | 46 | 8.06 |
| 629-605 | 100 | 236 | $6\times10^3$ | 160 | 1103 | 31 | 5.43 |
| -609 | 100 | 236 | $6\times10^3$ | 162 | 1117 | 37 | 6.48 |
| 630-610 | 140 | 236 | $6\times10^3$ | 117 | 807 | 9.0 | 1.58 |
| -611 | 140 | 236 | $6\times10^3$ | 144 | 993 | 23 | 4.03 |
| 631-610 | 140 | 236 | $6\times10^3$ | 117 | 807 | 9.0 | 1.58 |
| -611 | 140 | 236 | $6\times10^3$ | 144 | 993 | 17 | 2.98 |
| 115-116 | 22 | 0.33 | 8.3 | 443 | 3054 | 95 | 16.6 |
| -117 | 22 | 0.33 | 8.3 | 307 | 2117 | 58 | 10.2 |
| -118 | 22 | 0.33 | 8.3 | 280 | 1931 | 53 | 9.28 |
| 123-124 | 60 | 0.33 | 8.3 | 171 | 1179 | 33 | 5.78 |
| -125 | 60 | 0.33 | 8.3 | 157 | 1082 | 28 | 4.90 |
| -132 | 60 | 0.33 | 8.3 | 159 | 1096 | 29 | 5.08 |
| 135-133 | 100 | 0.33 | 8.3 | 117 | 807 | 10.3 | 1.80 |
| -134 | 100 | 0.33 | 8.3 | 109 | 752 | 8.4 | 1.47 |
| -308 | 100 | 0.33 | 8.3 | 126 | 869 | 11.3 | 1.98 |
| 149-150 | 140 | 0.33 | 8.3 | 99 | 683 | 6.1 | 1.07 |
| -151 | 140 | 0.33 | 8.3 | 93 | 641 | 5.4 | 0.95 |
| -152 | 140 | 0.33 | 8.3 | 87 | 600 | 4.6 | 0.81 |
| 224-209 | 22 | $6.6\times10^{-4}$ | $17\times10^{-3}$ | 211 | 1455 | 11.3 | 1.98 |
| -210 | 22 | $6.6\times10^{-4}$ | $17\times10^{-3}$ | 216 | 1489 | 11.6 | 2.03 |

TABLE 4. Tearing Energy Data for SER-20. All Tests Performed at a Crosshead Rate of 0.33 in./s (8.33 mm/s).

| Test Numbers | $T_s$, °C | Failure Stress | | Tearing Energy | |
|---|---|---|---|---|---|
| | | psi | MPa | in.-lb/in.$^2$ | J/m$^2$, $10^3$ |
| 370-352 | -20 | 492 | 3392 | 92 | 16.1 |
| -355 | -20 | 471 | 3247 | 68 | 11.9 |
| -358 | -20 | 478 | 3296 | 76 | 13.3 |
| 381-352 | -20 | 492 | 3392 | 99 | 17.3 |
| -355 | -20 | 471 | 3247 | 75 | 13.1 |
| -358 | -20 | 478 | 3296 | 81 | 14.2 |
| 364-313 | 22 | 390 | 2689 | 71 | 12.4 |
| -314 | 22 | 389 | 2682 | 71 | 12.4 |
| -325 | 22 | 412 | 2841 | 78 | 13.7 |
| 328-319 | 60 | 331 | 2282 | 52 | 9.11 |
| -331 | 60 | 296 | 2041 | 48 | 8.41 |
| -334 | 60 | 292 | 2013 | 46 | 8.06 |
| 380-319 | 60 | 331 | 2282 | 51 | 8.93 |
| -331 | 60 | 296 | 2041 | 47 | 8.23 |
| -334 | 60 | 292 | 2013 | 45 | 7.88 |
| 375-319 | 60 | 331 | 2282 | 70 | 12.3 |
| -331 | 60 | 296 | 2041 | 66 | 11.6 |
| -334 | 60 | 292 | 2013 | 62 | 10.9 |
| 361-322 | 100 | 250 | 1724 | 38 | 6.66 |
| -337 | 100 | 213 | 1469 | 26 | 4.55 |
| -340 | 100 | 212 | 1462 | 26 | 4.55 |
| 367-343 | 140 | 141 | 972 | 12 | 2.10 |
| -346 | 140 | 148 | 1020 | 15 | 2.63 |
| -349 | 140 | 142 | 979 | 12 | 2.10 |

TABLE 5. Tearing Energy Data for SBR-25. All Tests Performed at a Crosshead Rate of 0.33 in./s (8.33 mm/s).

| Test Numbers | T, °C | Failure Stress psi | Failure Stress MPa | Tearing Energy in.-lb/in.$^2$ | Tearing Energy J/m$^2$, $10^3$ |
|---|---|---|---|---|---|
| 371-353 | -20 | 649 | 4475 | 105 | 18.4 |
| -356 | -20 | 634 | 4371 | 94 | 16.5 |
| -359 | -20 | 625 | 4309 | 84 | 14.7 |
| 311-315 | 22 | 591 | 4075 | 102 | 17.9 |
| -316 | 22 | 580 | 3999 | 94 | 16.5 |
| -326 | 22 | 569 | 3923 | 87 | 15.2 |
| 329-320 | 60 | 556 | 3834 | 91 | 15.9 |
| -332 | 60 | 683 | 4709 | 121 | 21.2 |
| -335 | 60 | 555 | 3827 | 91 | 15.9 |
| 362-323 | 100 | 557 | 3840 | 100 | 17.5 |
| -338 | 100 | 683 | 4709 | 104 | 18.2 |
| -341 | 100 | 624 | 4302 | 102 | 17.9 |
| 368-344 | 140 | 507 | 3496 | 81 | 14.2 |
| 347 | 140 | 512 | 3530 | 88 | 15.4 |
| 350 | 140 | 502 | 3461 | 79 | 13.8 |
| 376-344 | 140 | 507 | 3496 | 85 | 14.9 |
| 347 | 140 | 512 | 3530 | 89 | 15.6 |
| 350 | 140 | 502 | 3461 | 84 | 14.7 |

TABLE 6. Tearing Energy Data for SBR-30. All Tests Performed at a Crosshead Rate of 0.33 in./s (8.33 mm/s).

| Test Numbers | T, °c | Failure Stress psi | Failure Stress MPa | Tearing Energy in.-lb/in.$^2$ | Tearing Energy J/m$^2$, $10^3$ |
|---|---|---|---|---|---|
| 391-392 | -20 | 690 | 4757 | 89 | 15.6 |
| 382-383 | 22 | 595 | 4102 | 89 | 15.6 |
| 384-385 | 60 | 582 | 4013 | 86 | 15.2 |
| 386-388 | 100 | 660 | 4551 | 114 | 20.0 |
| 389-390 | 140 | 731 | 5040 | 133 | 23.0 |

TABLE 7. Tearing Energy Data for SBR-35

| Test Numbers | T, °C | Cross-head Rate | | Failure Stress | | Tearing Energy | |
|---|---|---|---|---|---|---|---|
| | | in./s | mm/s | psi | MPa | in.-lb/in.$^2$ | J/m$^2$,10$^3$ |
| 227-217 | 22 | 236 | $6\times10^3$ | 2241 | 15,451 | 383 | 67.1 |
| -218 | 22 | 236 | $6\times10^3$ | 2091 | 13,921 | 369 | 64.6 |
| 228-217 | 22 | 236 | $6\times10^3$ | 2241 | 15,451 | 344 | 60.3 |
| -218 | 22 | 236 | $6\times10^3$ | 2091 | 13,921 | 320 | 56.0 |
| 620-612 | 60 | 236 | $6\times10^3$ | 761 | 5247 | 574 | 100.5 |
| -613 | 60 | 236 | $6\times10^3$ | 672 | 4633 | 416 | 72.9 |
| 632-612 | 60 | 236 | $6\times10^3$ | 761 | 5247 | 551 | 96.5 |
| -613 | 60 | 236 | $6\times10^3$ | 672 | 4633 | 466 | 81.6 |
| 633-614 | 100 | 236 | $6\times10^3$ | 433 | 2985 | 326 | 57.1 |
| -615 | 100 | 236 | $6\times10^3$ | 395 | 2723 | 293 | 51.3 |
| 634-614 | 100 | 236 | $6\times10^3$ | 433 | 2985 | 164 | 28.7 |
| -615 | 100 | 236 | $6\times10^3$ | 395 | 2723 | 129 | 22.6 |
| 635-616 | 140 | 236 | $6\times10^3$ | 343 | 2344 | 66 | 11.6 |
| -617 | 140 | 236 | $6\times10^3$ | 337 | 2344 | 65 | 11.4 |
| 636-616 | 140 | 236 | $6\times10^3$ | 343 | 2344 | 98 | 17.2 |
| -617 | 140 | 236 | $6\times10^3$ | 337 | 2344 | 96 | 16.8 |
| 112-108 | 22 | 0.33 | 8.3 | 719 | 4957 | 92 | 16.1 |
| -109 | 22 | 0.33 | 8.3 | 826 | 5695 | 112 | 19.6 |
| -110 | 22 | 0.33 | 8.3 | 659 | 4544 | 68 | 11.9 |
| 113 | 22 | 0.33 | 8.3 | 742 | 5116 | 89 | 15.6 |
| 128-126 | 60 | 0.33 | 8.3 | 921 | 6350 | 163 | 28.5 |
| -127 | 60 | 0.33 | 8.3 | 687 | 4737 | 101 | 17.7 |
| -307 | 60 | 0.33 | 8.3 | 871 | 6005 | 140 | 24.5 |
| 137-136 | 100 | 0.33 | 8.3 | 685 | 4723 | 83 | 14.5 |
| -153 | 100 | 0.33 | 8.3 | 767 | 5288 | 118 | 20.7 |
| -309 | 100 | 0.33 | 8.3 | 998 | 6881 | 158 | 27.7 |
| 148-146 | 140 | 0.33 | 8.3 | 287 | 1979 | 27 | 4.72 |
| -147 | 140 | 0.33 | 8.3 | 500 | 3447 | 67 | 11.7 |
| -230 | 140 | 0.33 | 8.3 | 545 | 3758 | 72 | 12.6 |
| 220-211* | 22 | $6.6\times10^{-4}$ | $17\times10^{-3}$ | 1558 | 10,742 | 292 | 51.1 |
| -219 | 22 | $6.6\times10^{-4}$ | $17\times10^{-3}$ | 1000 | 6895 | 193 | 33.8 |

*Test 211 pulled at cross-head rate of $3.3 \times 10^{-4}$ in/s.

TABLE 8. Tearing Energy Data for SBR-40. All Tests Performed at a Crosshead Rate of 0.33 in./s (8.33 mm/s).

| Test Numbers | T, °c | Failure Stress | | Tearing Energy | |
|---|---|---|---|---|---|
| | | psi | MPa | in.-lb/in.$^2$ | J/m$^2$, $10^3$ |
| 272-354 | -20 | 739 | 5095 | 75 | 13.1 |
| -357 | -20 | 791 | 5454 | 77 | 13.5 |
| -360 | -20 | 785 | 5412 | 76 | 13.3 |
| 312-317 | 22 | 768 | 5295 | 128 | 22.4 |
| -318 | 22 | 795 | 5481 | 131 | 22.9 |
| -327 | 22 | 727 | 5013 | 111 | 19.4 |
| 379-317 | 22 | 768 | 5295 | 92 | 16.1 |
| -318 | 22 | 795 | 5481 | 94 | 16.5 |
| -327 | 22 | 727 | 5013 | 79 | 13.8 |
| 330-321 | 60 | 796 | 5488 | 103 | 18.0 |
| -333 | 60 | 684 | 4716 | 76 | 13.3 |
| -336 | 60 | 642 | 4426 | 76 | 13.3 |
| 363-324 | 100 | 583 | 4020 | 65 | 11.4 |
| -339 | 100 | 552 | 3806 | 55 | 9.63 |
| -342 | 100 | 593 | 4089 | 65 | 11.4 |
| 369-345 | 140 | 427 | 2944 | 45 | 7.88 |
| -348 | 140 | 418 | 2882 | 46 | 8.06 |
| -351 | 140 | 461 | 3179 | 44 | 7.88 |

TABLE 9. Tearing Energy Data for T142 Goodyear Pads-115 and -145 and T156 Goodyear Pad. All Tests Performed at a Crosshead Rate of 0.33 in./s (8.33 mm/s).

| | | | Failure Stress | | Tearing Energy | |
|---|---|---|---|---|---|---|
| Test Number | Layer | T, °C | psi | MPa | in.-lb/in.$^2$ | J/m$^2$, $10^3$ |
| 11 | A | 22* | 950 | 6550 | 137 | 24.0 |
| -7 | A | 22* | 970 | 6688 | 142 | 24.9 |
| -8 | E | 22* | 1030 | 7102 | 157 | 27.5 |
| -9 | E | 22* | 990 | 6826 | 150 | 26.3 |
| 64-58 | C | 60* | 1120 | 772? | 177 | 13.0 |
| -60 | D | 60* | 1090 | 7515 | 172 | 30.1 |
| -61 | B | 60* | 1090 | 7515 | 169 | 29.6 |
| -62 | C | 60* | 1075 | 7412 | 163 | 28.5 |
| 70-50 | D | 100+ | 900 | 6205 | 147 | 25.7 |
| -51 | D | 100+ | 665 | 4585 | 95 | 16.6 |
| 42 | D | 100+ | 567 | 3909 | 70 | 12.3 |
| 71-38 | A | 140+ | 571 | 3937 | 87 | 15.2 |
| -39 | A | 140+ | 380 | 2620 | 44 | 7.71 |
| -40 | A | 140+ | 439 | 3027 | 55 | 9.63 |
| -41 | F | 140+ | 538 | 3709 | 79 | 13.8 |
| 25-21 | A | 22# | 892 | 6150 | 144 | 24.7 |
| -22 | A | 22# | 868 | 5985 | 132 | 23.1 |
| -23 | C | 22# | 735 | 5068 | 100 | 17.5 |
| -24 | C | 22# | 735 | 5068 | 100 | 17.5 |
| 76-46 | B | 140# | 345 | 2379 | 43 | 7.53 |
| -47 | B | 140# | 391 | 2696 | 62 | 10.9 |
| -48 | D | 140# | 482 | 3323 | 71 | 12.4 |
| -49 | D | 140# | 430 | 2965 | 67 | 11.7 |

*G-T142-145; +G-T142-115; #G-T156.

**TABLE 10. Tearing Energy Data for T142 Firestone Pad-117 and T156 Firestone Pad. All Tests Performed at a Crosshead Rate of 0.33 in./s (8.33 mm/s).**

| Test Number | Layer | T, °C | Failure Stress psi | Failure Stress MPa | Tearing Energy in.-lb/in.$^2$ | Tearing Energy J/m$^2$, $10^3$ |
|---|---|---|---|---|---|---|
| 1-2 | A | 22* | 790 | 5447 | 102 | 17.9 |
| -3 | A | 22* | 880 | 6067 | 111 | 19.4 |
| -4 | H | 22* | 1145 | 7895 | 168 | 29.4 |
| -5 | H | 22* | 1130 | 7791 | 153 | 26.8 |
| 65-55 | E | 60* | 983 | 6778 | 186 | 32.6 |
| -57 | B | 60* | 660 | 4551 | 79 | 13.8 |
| -58 | C | 60* | 824 | 5681 | 104 | 18.2 |
| 67-53 | G | 100* | 900 | 6205 | 129 | 22.6 |
| -54 | G | 100* | 941 | 6488 | 136 | 23.8 |
| -68 | C | 100* | 687 | 4737 | 90 | 15.8 |
| 74-42 | D | 140* | 550 | 3792 | 70 | 12.3 |
| -43 | D | 140* | 555 | 3827 | 71 | 12.4 |
| -44 | G | 140* | 531 | 3661 | 66 | 11.6 |
| -45 | D | 140* | 582 | 4013 | 67 | 13.5 |
| 77-88 | C | 22+ | 1330 | 9170 | 192 | 33.6 |
| -89 | C | 22+ | 941 | 6488 | 114 | 20.0 |
| 92-103 | D | 140+ | 280 | 1931 | 31 | 5.43 |
| -104 | D | 140+ | 250 | 1724 | 20 | 3.50 |
| -105 | D | 140+ | 495 | 3413 | 85 | 14.9 |
| 93-106 | B | 140+ | 555 | 3827 | 87 | 15.2 |
| -107 | B | 140+ | 440 | 3034 | 88 | 10.2 |

*F-T142-117; +F-T156

TABLE 11. Tearing Energy Data for T156 Standard Pad and T156 Standard Pad-380. All Tests Performed at a Crosshead Rate of 0.33 in./s (8.33 mm/s).

| Test Number | Layer | T, °C | Failure Stress psi | Failure Stress MPa | Tearing Energy in.-lb/in.$^2$ | Tearing Energy J/m$^2$, $10^3$ |
|---|---|---|---|---|---|---|
| 81-84 | C | 22* | 1110 | 7653 | 183 | 32.1 |
| -85 | C | 22* | 968 | 6674 | 151 | 26.4 |
| 78-86 | E | 22* | 1050 | 7240 | 167 | 29.3 |
| -87 | E | 22* | 1040 | 7171 | 162 | 28.4 |
| 94-99 | D | 140* | 600 | 4137 | 93 | 16.3 |
| -100 | D | 140* | 465 | 3206 | 65 | 11.4 |
| 77-82 | E | 22+ | 645 | 4447 | 87 | 15.2 |
| -83 | E | 22+ | 616 | 4247 | 80 | 14.0 |
| -90 | C | 22+ | 842 | 5804 | 114 | 20.0 |
| -91 | C | 22+ | 655 | 4516 | 83 | 14.5 |
| 95-97 | D | 140+ | 460 | 3172 | 67 | 11.7 |
| -98 | D | 140+ | 360 | 2482 | 42 | 7.36 |
| -101 | B | 140+ | 303 | 2089 | 29 | 5.08 |
| -102 | B | 140+ | 470 | 3241 | 51 | 8.93 |

*S-T156; +S-T156-380

**TABLE 12. Relative Ratings on the Extent of Deviated, Knotty Tearing**

| Formulation | T, °C | Cross-head Rate, in./s | Test No. | Rating | |
|---|---|---|---|---|---|
| | | | | Sharp | Gradual |
| SBR-0 | all | all | all | 0 | 0 |
| SBR-15 | all | all | all | 0 | 0 |
| SBR-20 | -20 | 0.33 | all | 0 | 0 |
| SBR-20 | 22 | 0.33 | all | 0 | 0 |
| SBR-20 | 60 | 0.33 | all | 0 | 0 |
| SBR-20 | 100 | 0.33 | all | 0 | 0 |
| SBR-20 | 140 | 0.33 | 343,346 | 1 | |
| SBR-20 | 140 | 0.33 | 349 | 2 | |
| SBR-25 | -20 | 0.33 | all | 0 | 0 |
| SBR-25 | 22 | 0.33 | all | 0 | 0 |
| SBR-25 | 60 | 0.33 | all | 2 | |
| SBR-25 | 100 | 0.33 | 323,341 | 8 | |
| SBR-25 | 100 | 0.33 | 338 | 9 | |
| SBR-25 | 140 | 0.33 | 344 | 1 | |
| SBR-25 | 140 | 0.33 | 350 | 2 | |
| SBR-25 | 140 | 0.33 | 347 | 3 | |
| SBR-30 | -20 | 0.33 | 242 | 0 | 0 |
| SBR-30 | 22 | 0.33 | 383 | | 2 |
| SBR-30 | 60 | 0.33 | 385 | 4 | |
| SBR-30 | 100 | 0.33 | 388 | 2 | |
| SBR-30 | 140 | 0.33 | 390 | 7 | |
| SBR-35 | 22 | 235 | all | 0 | |
| SBR-35 | 60 | 235 | 612,613 | | 3 |
| SBR-35 | 100 | 235 | 614 | 0 | |
| SBR-35 | 100 | 235 | 615 | | 2 |
| SBR-35 | 140 | 235 | 616 | | 4 |
| SBR-35 | 140 | 235 | 617 | | 3 |
| SBR-35 | 22 | 0.33 | 108 | | 5 |
| SBR-35 | 22 | 0.33 | 109 | | 4 |
| SBR-35 | 22 | 0.33 | 110 | | 1 |
| SBR-35 | 22 | 0.33 | 113 | | 2 |
| SBR-35 | 60 | 0.33 | 126 | 8 | |
| SBR-35 | 60 | 0.33 | 127 | 5 | |
| SBR-35 | 60 | 0.33 | 307 | 7 | |
| SBR-35 | 100 | 0.33 | 136 | 8 | |
| SBR-35 | 100 | 0.33 | 153 | 9 | |
| SBR-35 | 100 | 0.33 | 309 | 1 | |
| SBR-35 | 140 | 0.33 | 146 | 10 | |
| SBR-35 | 140 | 0.33 | 147 | 7 | |
| SBR-35 | 140 | 0.33 | 230 | 6 | |
| SBR-35 | 22 | $3.3 \times 10^{-4}$ | 211 | 9 | |
| SBR-35 | 22 | $6.6 \times 10^{-4}$ | 219 | 8 1/2 | |

TABLE 12. Continued

| Formulation | T, °C | Cross-head Rate, in./s | Test No. | Rating | |
|---|---|---|---|---|---|
| | | | | Sharp | Gradual |
| SBR-40 | -20 | 0.33 | 354,318 | | 1 |
| SBR-40 | -20 | 0.33 | 360 | | 2 |
| SBR-40 | 22 | 0.33 | 317,318 | | 5 |
| SBR-40 | 22 | 0.33 | 327 | | 2 |
| SBR-40 | 60 | 0.33 | 321,336 | 7 | 7 |
| SBR-40 | 60 | 0.33 | 333 | 5 | 5 |
| SBR-40 | 100 | 0.33 | 324 | 7 | 7 |
| SBR-40 | 100 | 0.33 | 342,339 | 8 | 8 |
| SBR-40 | 140 | 0.33 | 345,351 | 8 | 8 |
| SBR-40 | 140 | 0.33 | 348 | 9 | 9 |

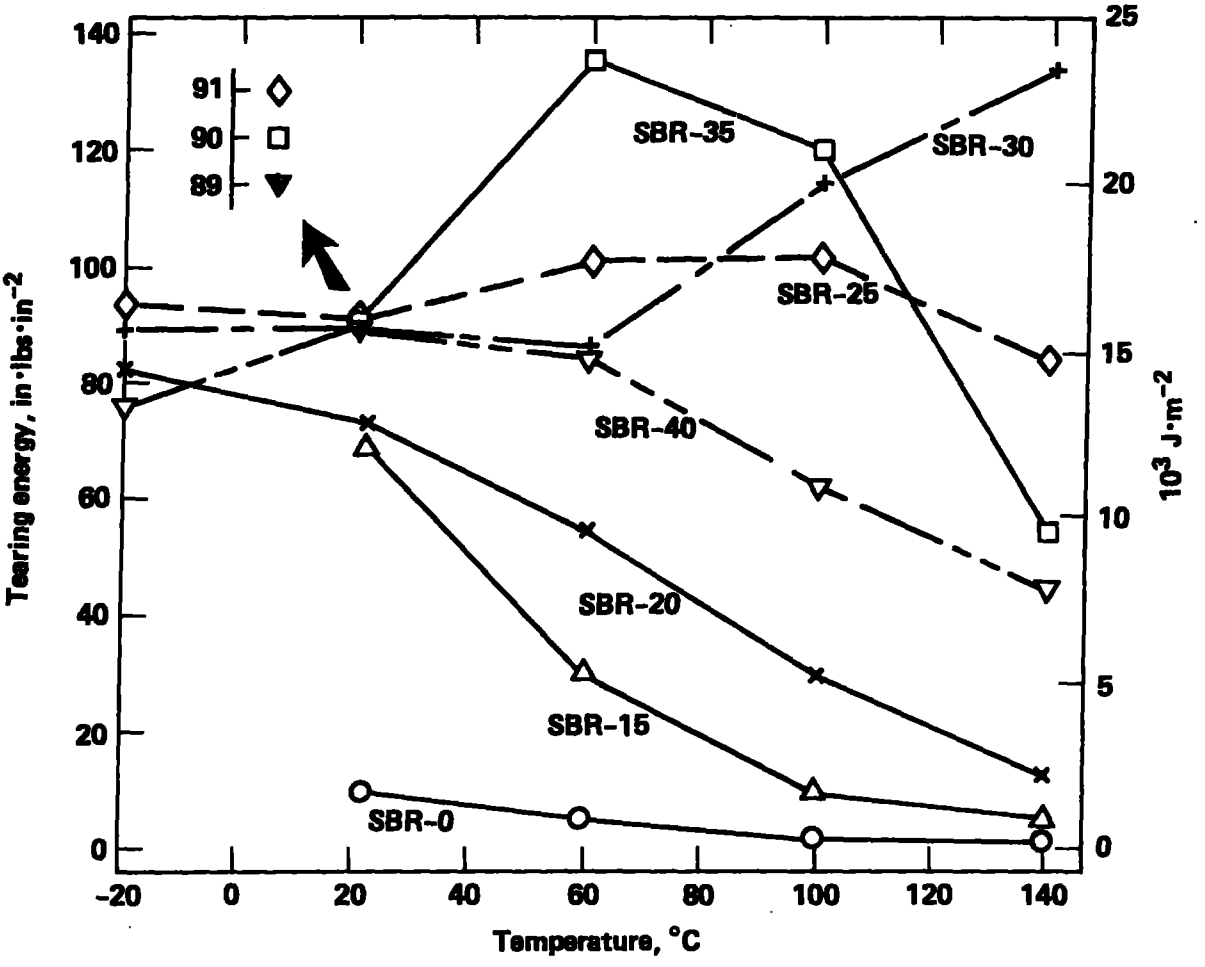


Fig. 1. Tearing energy as a function of temperature for a series of laboratory-formulated SBR elastomers tested at a crosshead rate of 0.33 in./s ($\dot{\varepsilon} \approx 10^{-1}$/s).

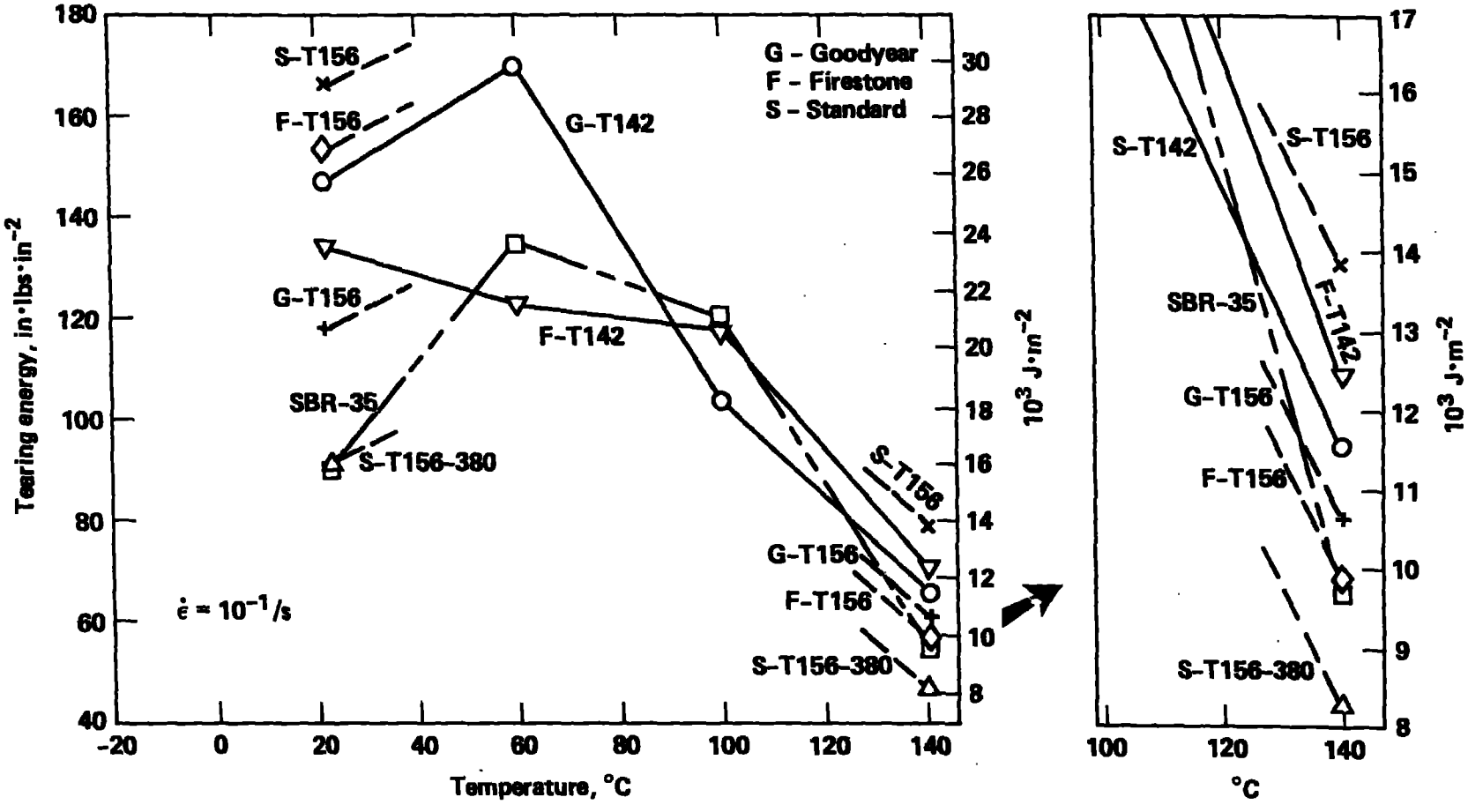


Fig. 2. Tearing energy as a function of temperature for samples removed from tank track pads. Samples tested at a crosshead rate of 0.33 in./s ($\dot{\epsilon} = 10^{-1}$/s). Results for SBR-35 are included.

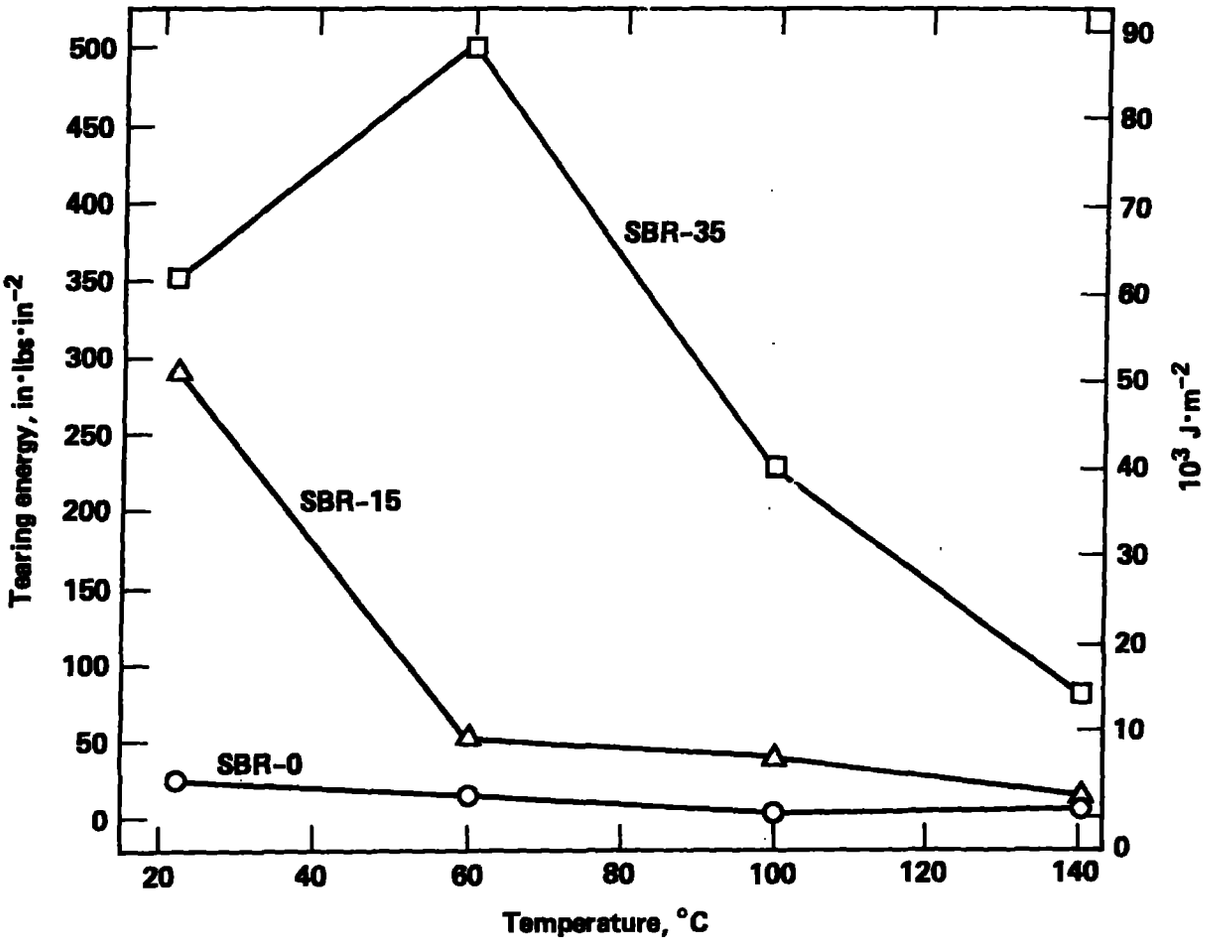


Fig. 3. Tearing energy as a function of temperature for three laboratory-formulated SBR elastomers tested at a high stroke-displacement rate of approx. 235 in./s ($\dot{\varepsilon} \approx 470/s$ for un-nicked samples).

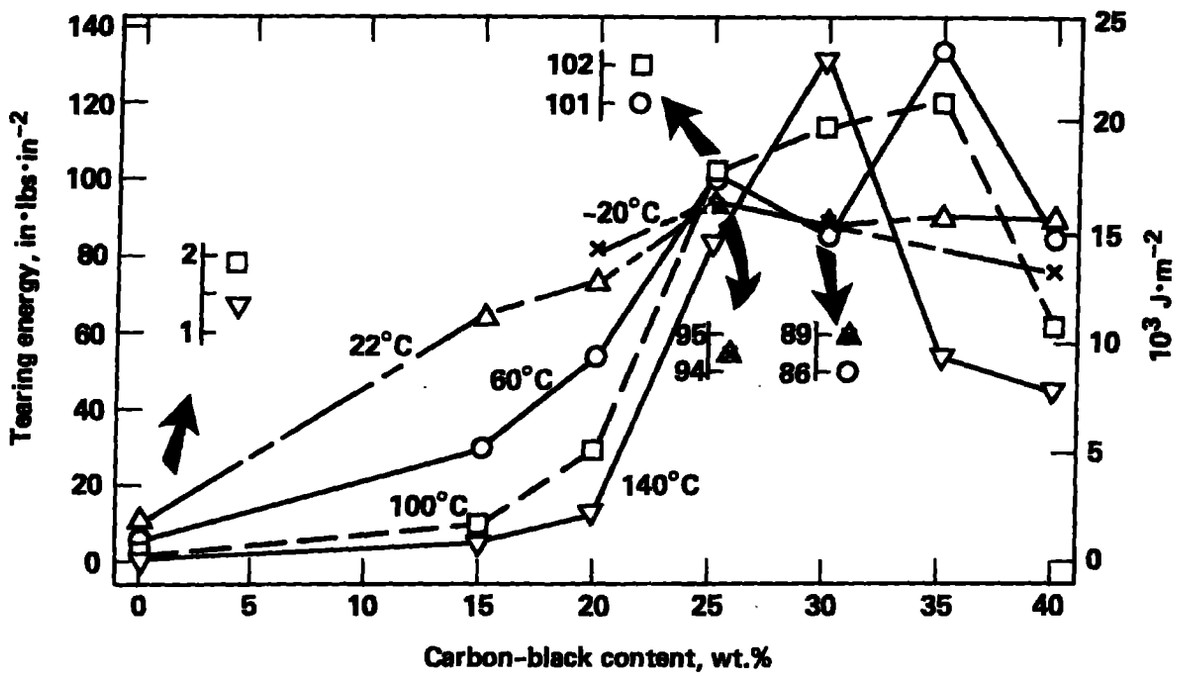


Fig. 4. Tearing energy as a function of carbon-black content. Samples tested at a stroke rate of 0.33 in./s ($\dot{\varepsilon} \approx 10^{-1}$/s) at five temperatures.

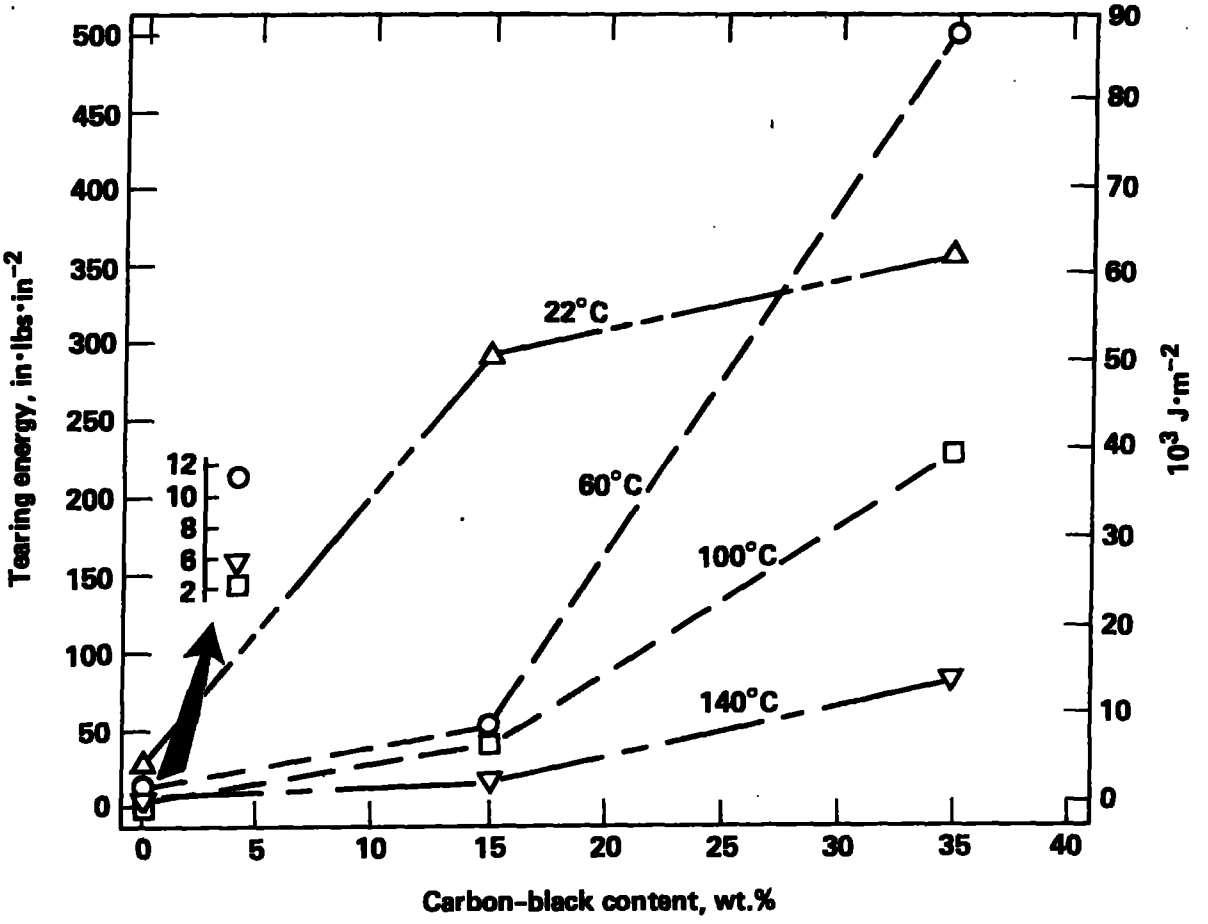


Fig. 5. Tearing energy as a function of carbon-black content. Samples tested at a stroke rate of 235 in./s ($\dot{\varepsilon} \approx 470$/s for un-nicked samples) at four temperatures.

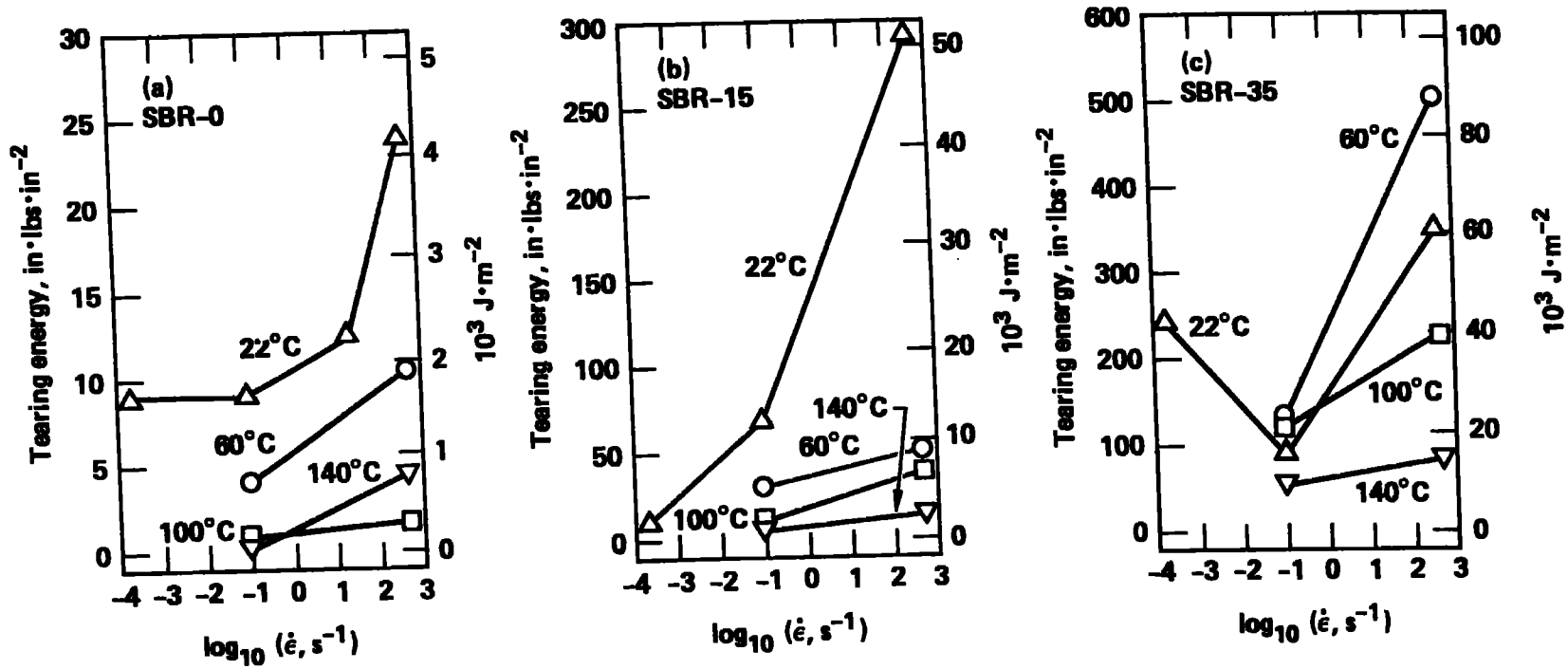


Fig. 6. Effect of strain rate on tearing energy at various temperatures for SBR-0, -15, and -35. (Strain rates are for un-nicked samples).

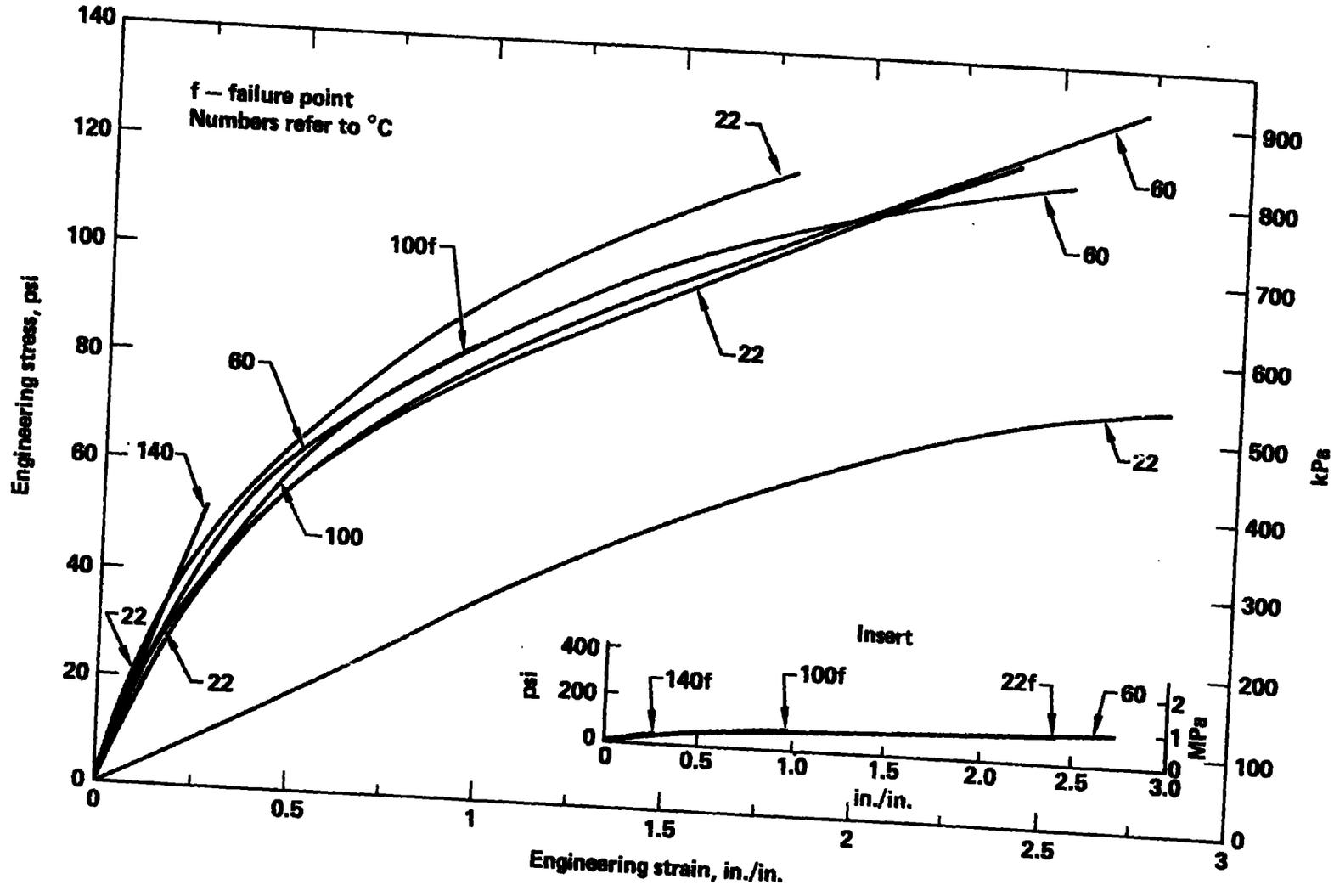


Fig. 7. Stress-strain curves for un-nicked SBR-0 strip samples tested at various temperatures at a crosshead rate of 0.33 in./s ($\dot{\varepsilon} \approx 10^{-1}$/s). Insert plotted on same scale used for stress-strain curves of remaining formulations.

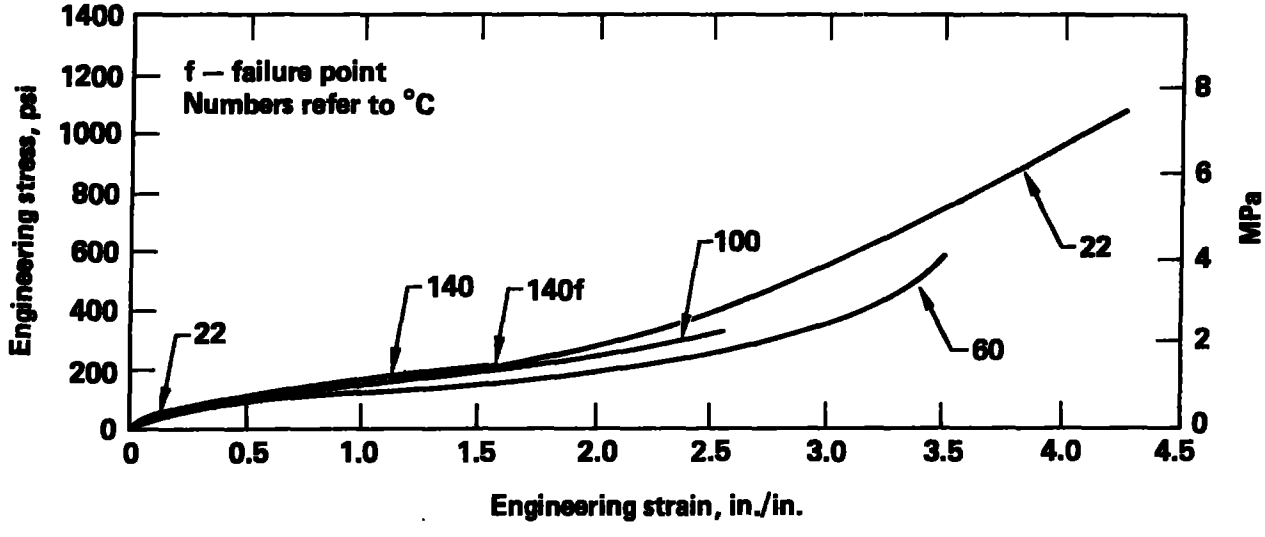


Fig. 8. Stress-strain curves for un-nicked SBR-15 strip samples tested at various temperatures at a crosshead rate of 0.33 in./s ($\dot{\varepsilon} \approx 10^{-1}$/s).

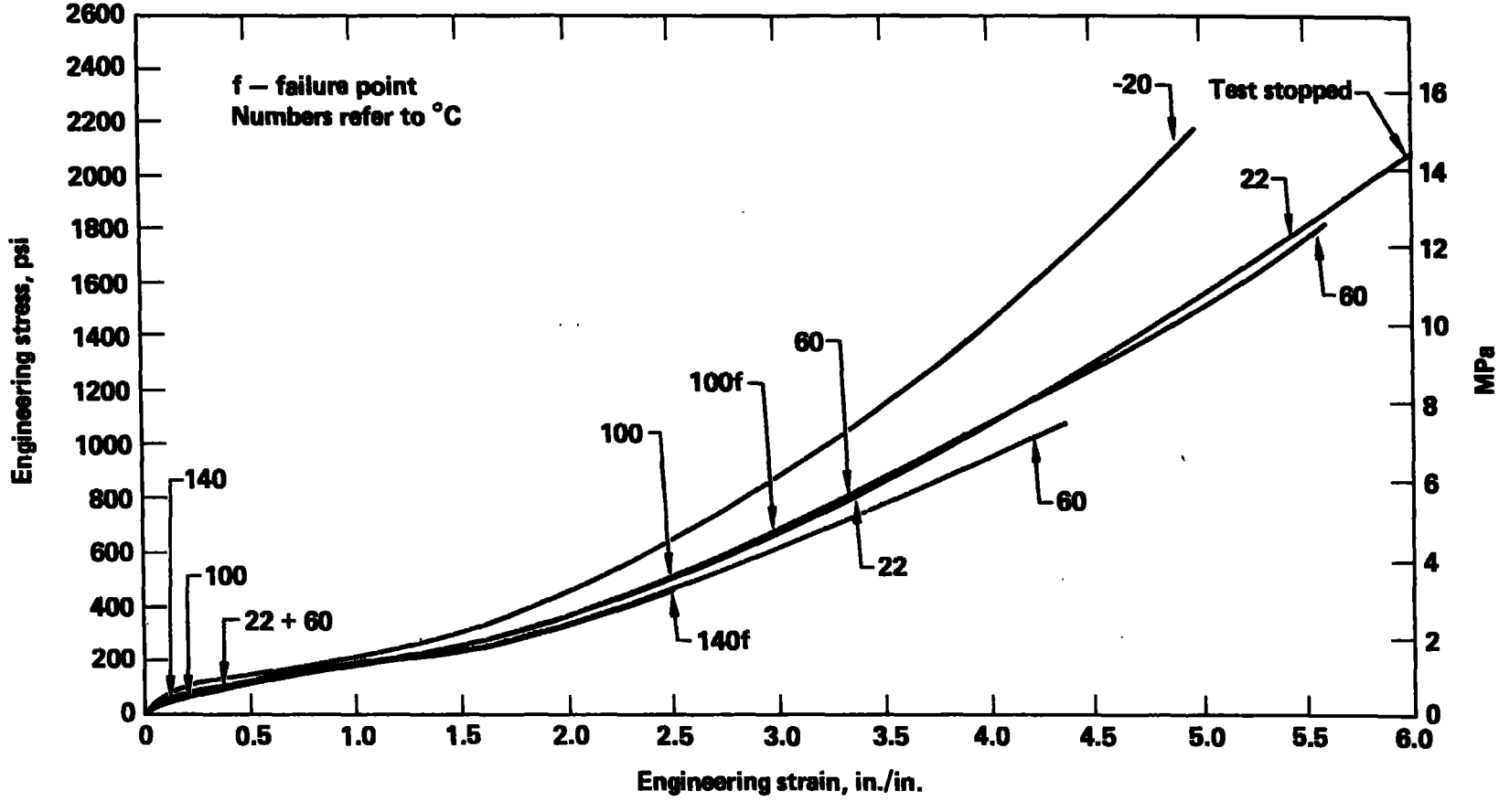


Fig. 9. Stress-strain curves for un-nicked SBR-20 strip samples tested at various temperatures at a crosshead rate of 0.33 in./s ($\dot{\varepsilon} \approx 10^{-1}$/s).

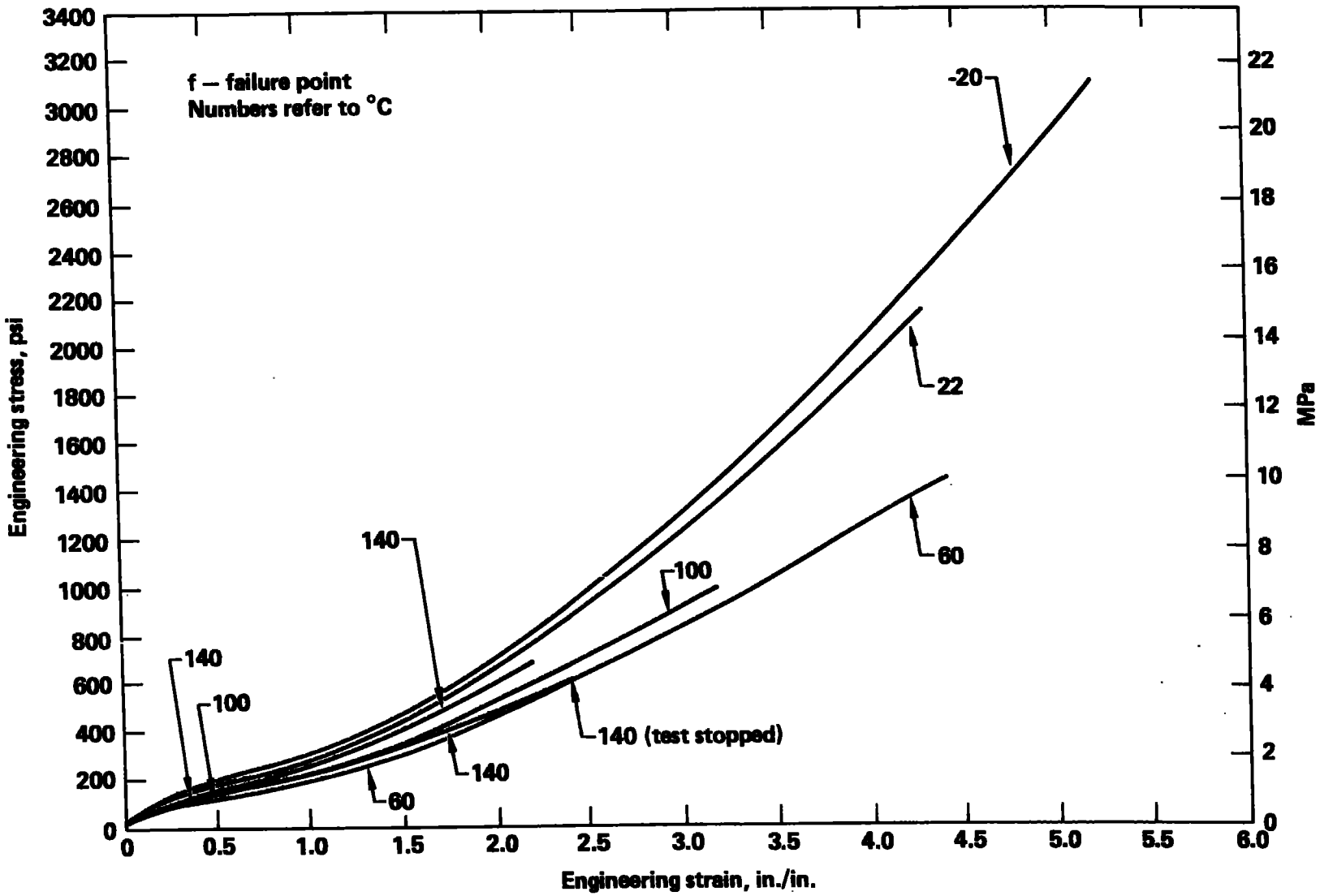


Fig. 10. Stress-strain curves for un-nicked SBR-25 strip samples tested at various temperatures at a crosshead rate of 0.33 in./s. ($\dot{\varepsilon} \approx 10^{-1}$/s).

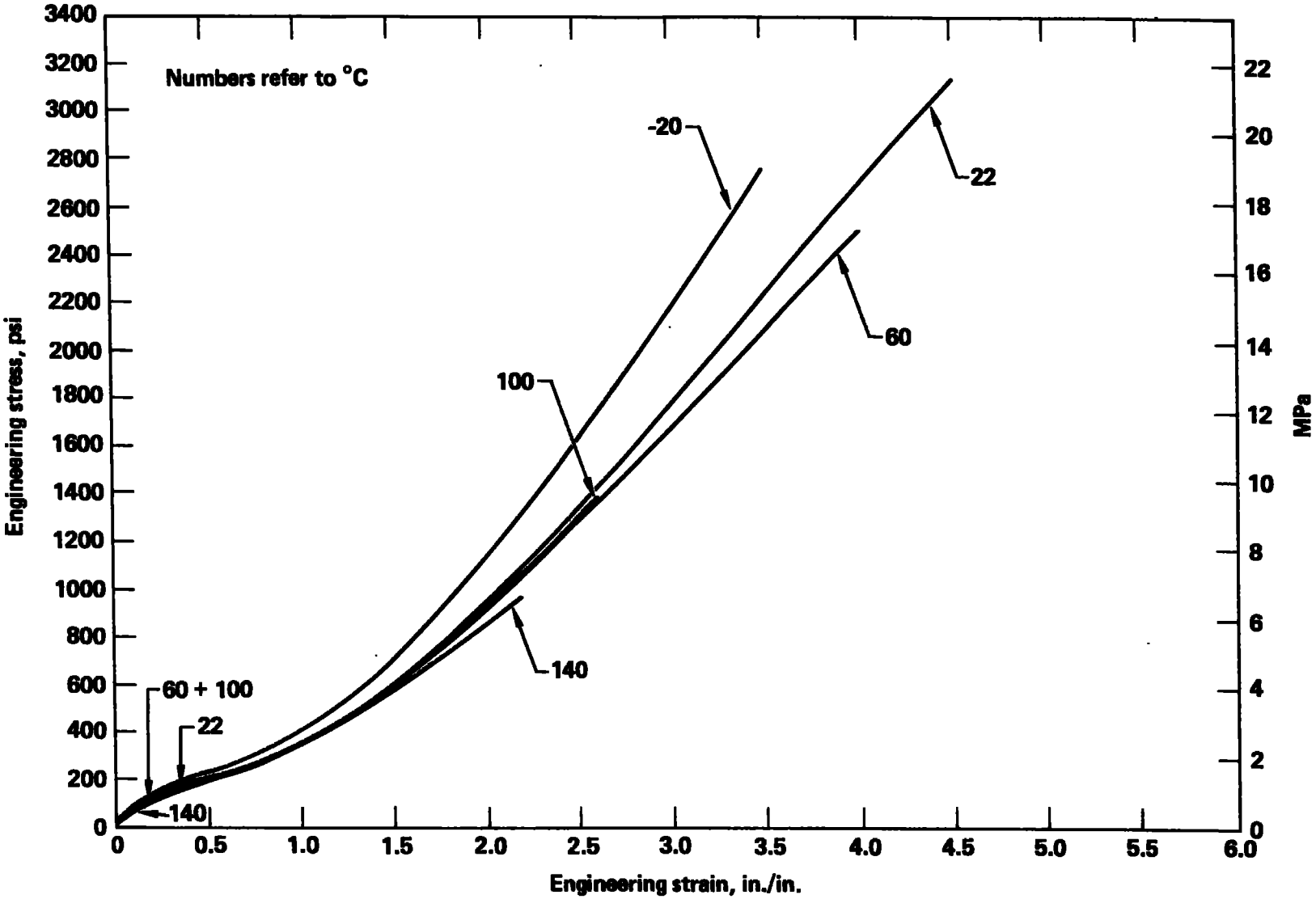


Fig. 11. Stress-strain curves for un-nicked SBR-30 strip samples tested at various temperatures at a crosshead rate of 0.33 in./s ($\dot{\varepsilon} \approx 10^{-1}$/s).

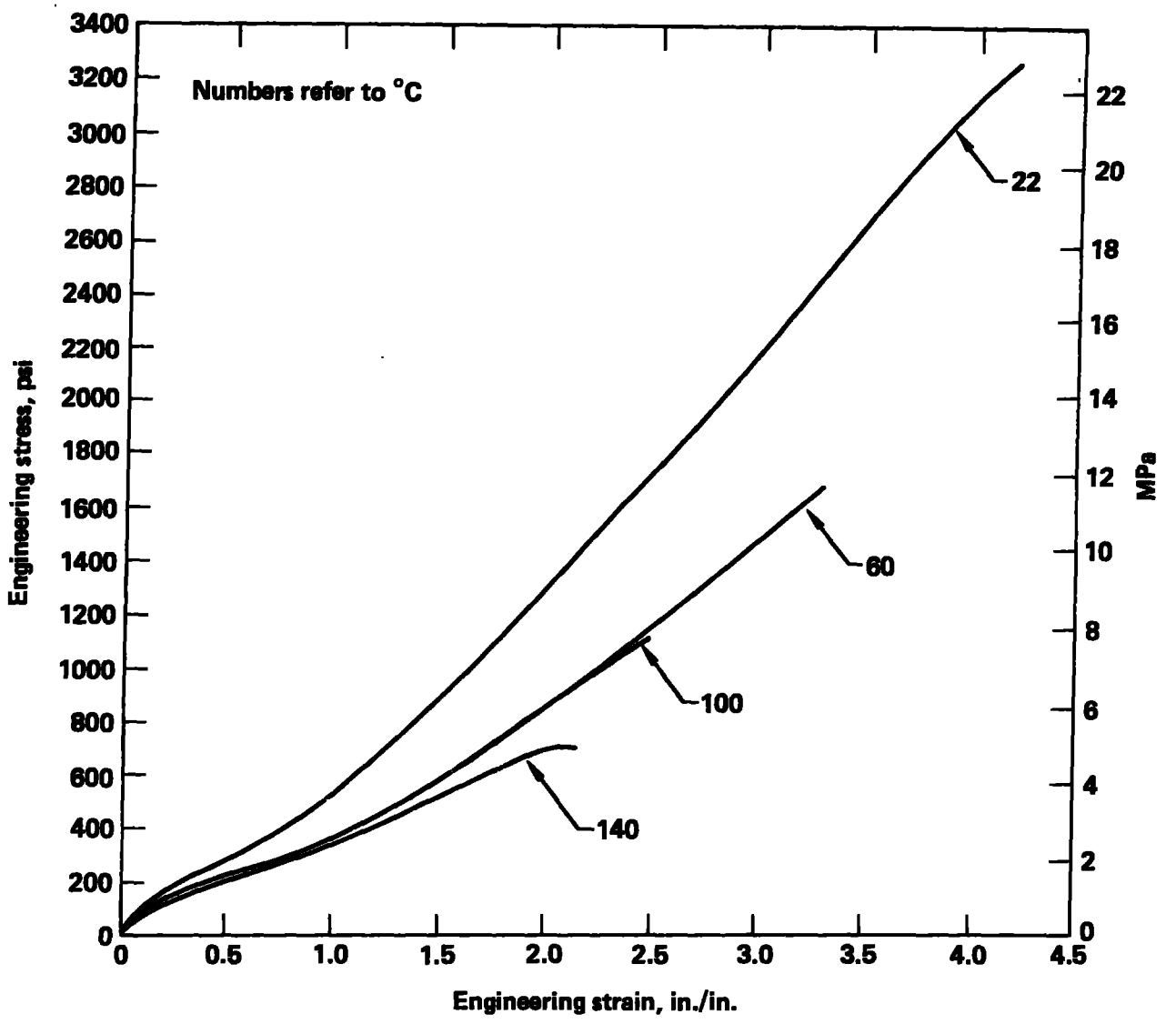


Fig. 12. Stress-strain curves for un-nicked SBR-35 strip samples tested at various temperatures at a crosshead rate of 0.33 in./s ($\dot{\varepsilon} \approx 10^{-1}$/s).

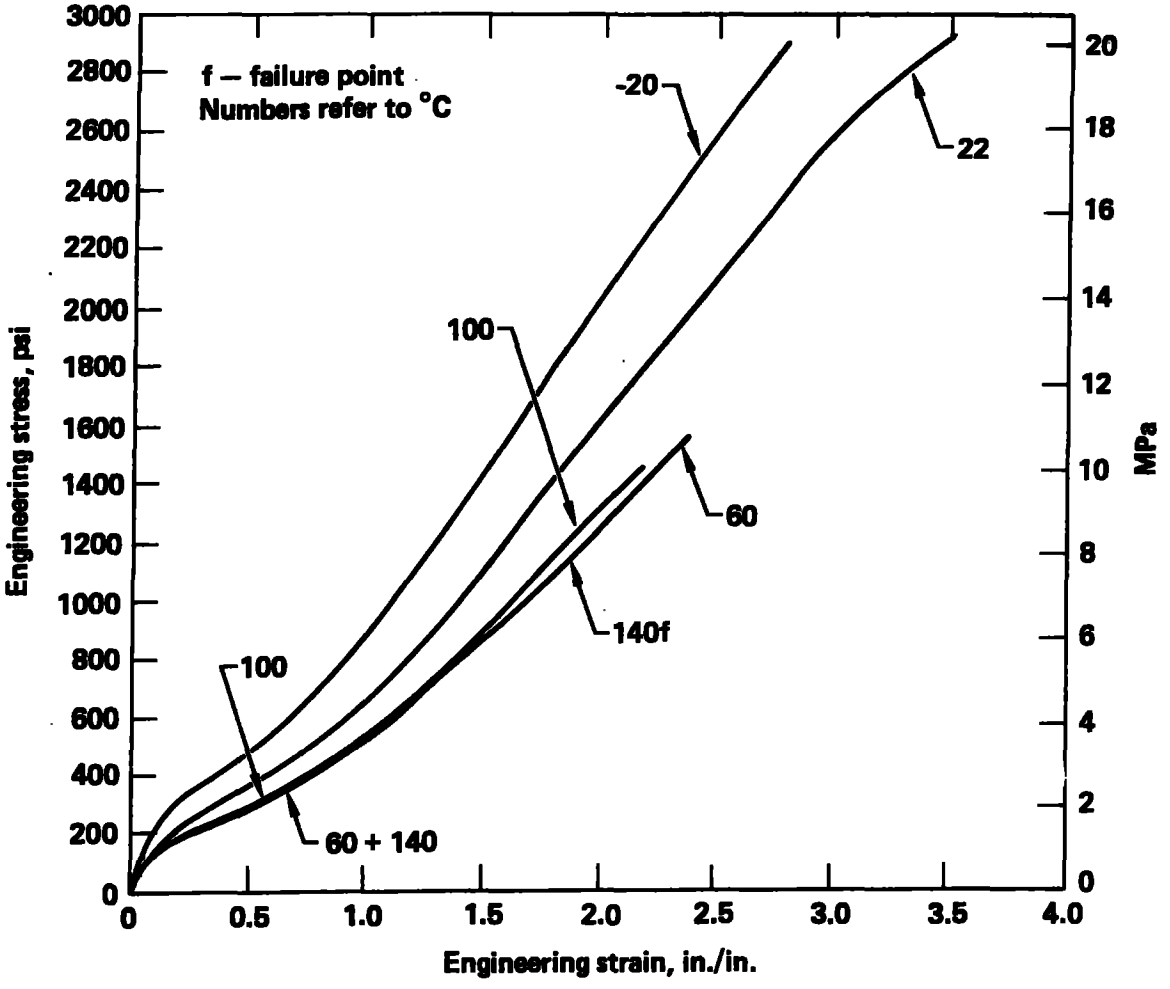


Fig. 13. Stress-strain curves for un-nicked SBR-40 strip samples tested at various temperatures at a crosshead rate of 0.33 in./s ($\dot{\varepsilon} \approx 10^{-1}$/s).

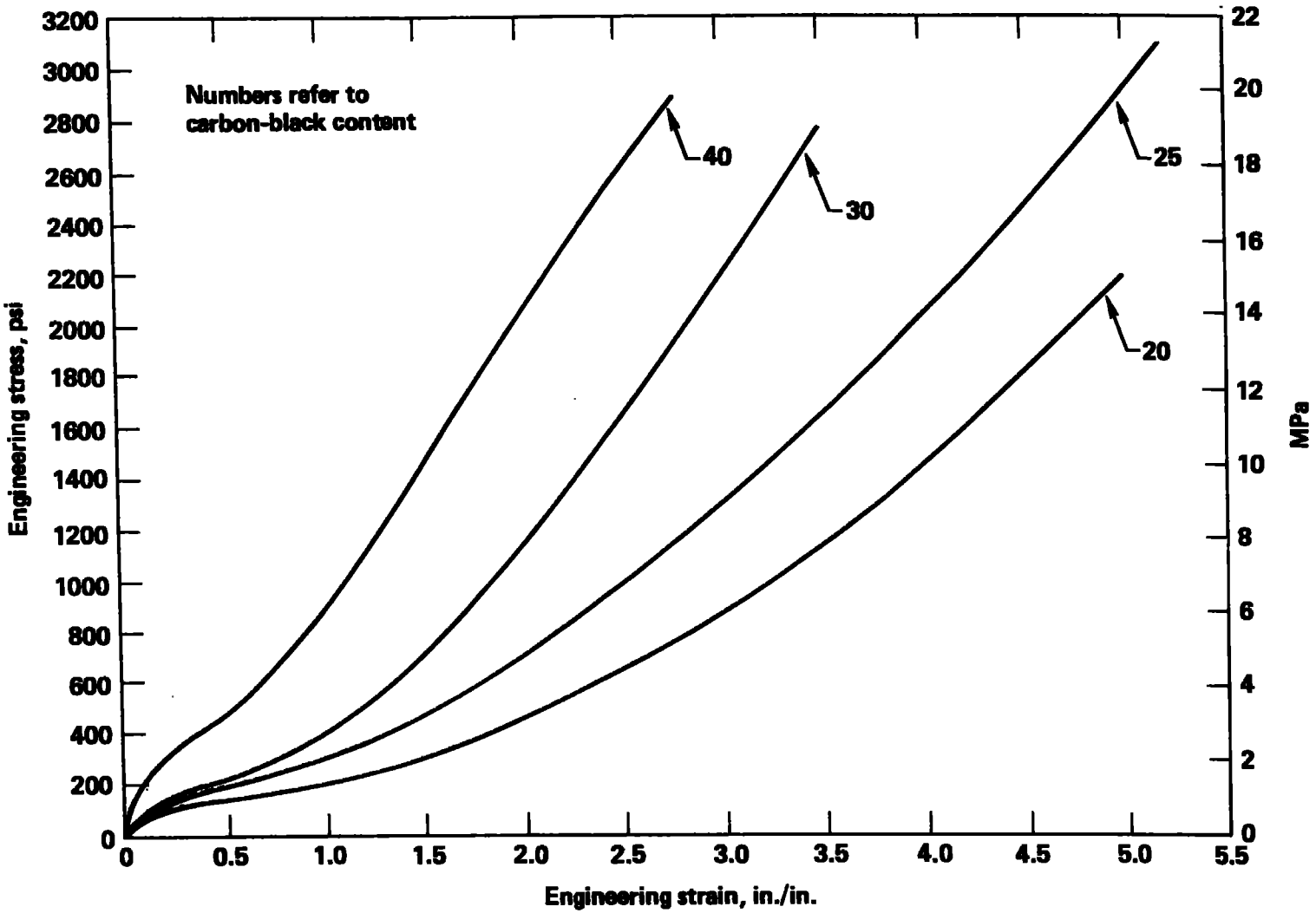


Fig. 14. Stress-strain curves for un-nicked SBR strip samples tested at -20° C at a crosshead rate of 0.33 in./s ($\dot{\varepsilon} \approx 10^{-1}$/s).

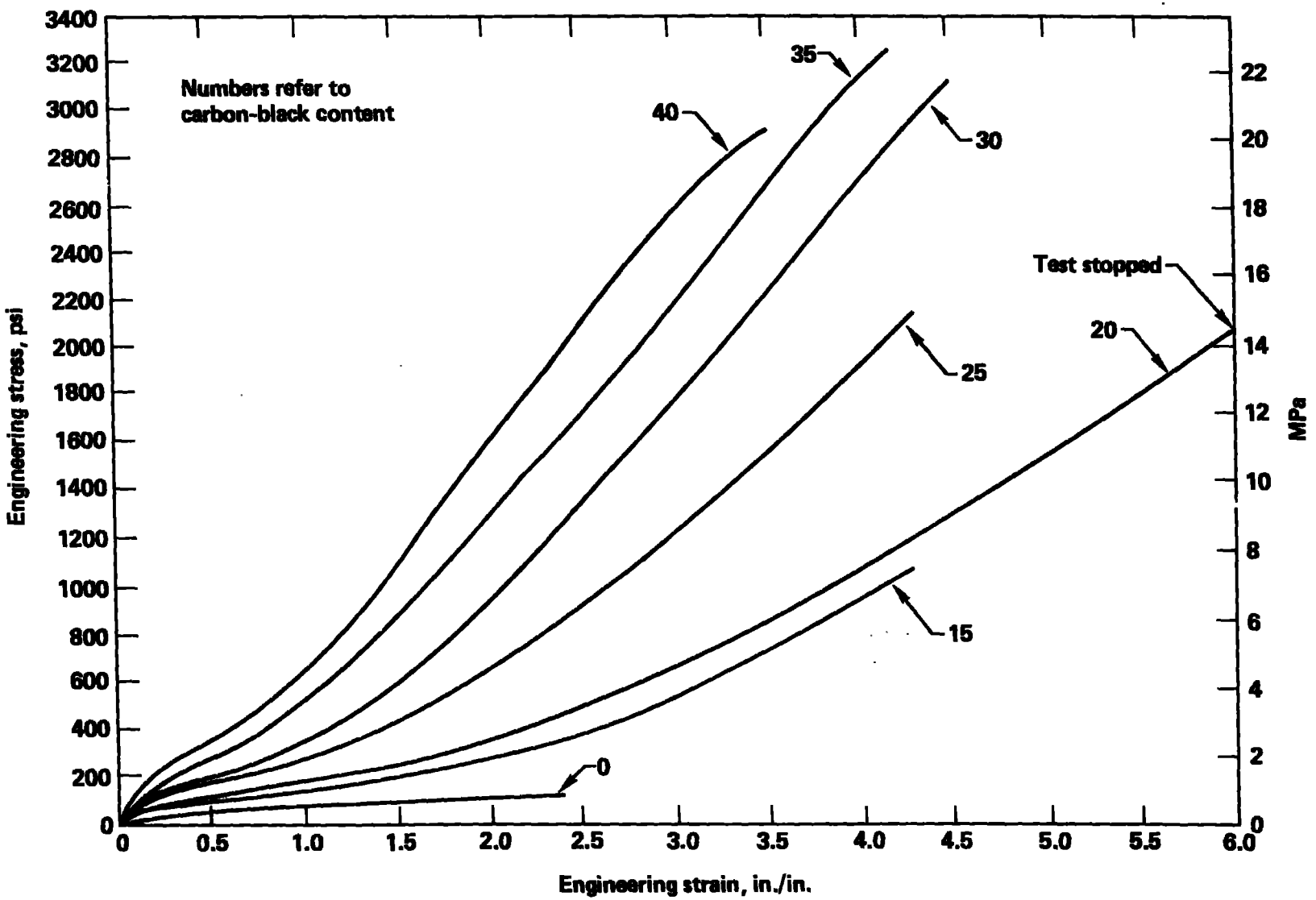


Fig. 15. Stress strain curves for un-nicked SBR strip samples tested at 22° C at a crosshead rate of 0.33 in./s ($\dot{\varepsilon} \approx 10^{-1}$/s).

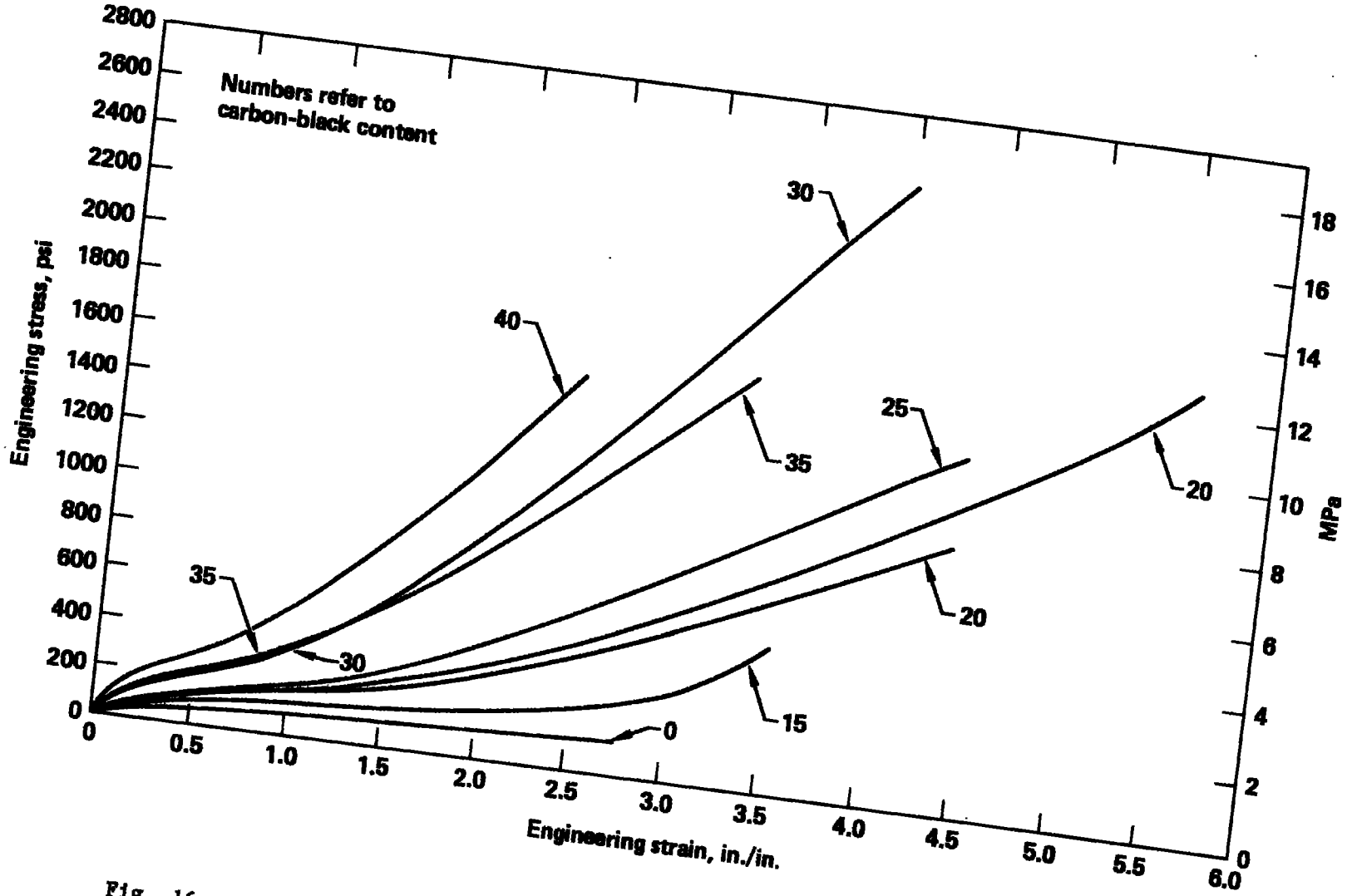


Fig. 16. Stress-strain curves for un-nicked SBR strip samples tested at 60° C at a crosshead rate of 0.33 in./s ($\dot{\varepsilon} \approx 10^{-1}$/s).

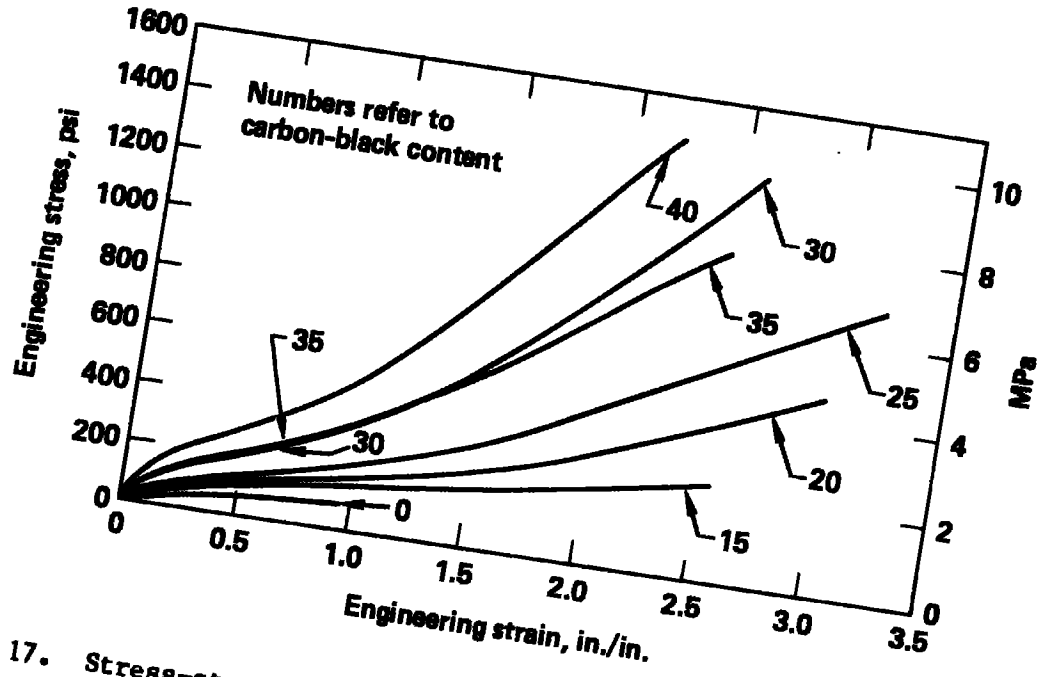


Fig. 17. Stress-strain curves for un-nicked SBR strip samples tested at 100° C at a crosshead rate of 0.33 in./s ($\dot{\varepsilon} \approx 10^{-1}$/s).

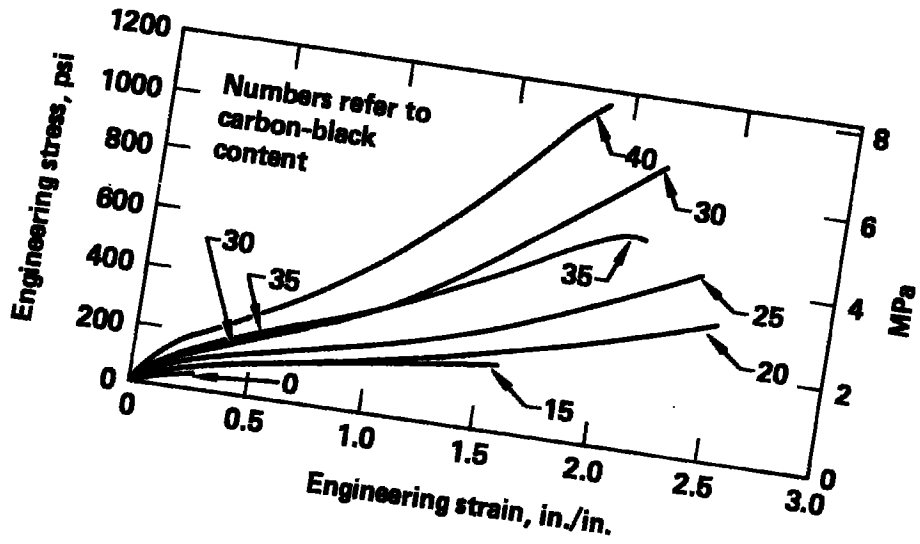


Fig. 18. Stress-strain curves for un-nicked SBR strip samples tested at 140° C at a crosshead rate of 0.33 in./s ($\dot{\varepsilon} \approx 10^{-1}$/s).

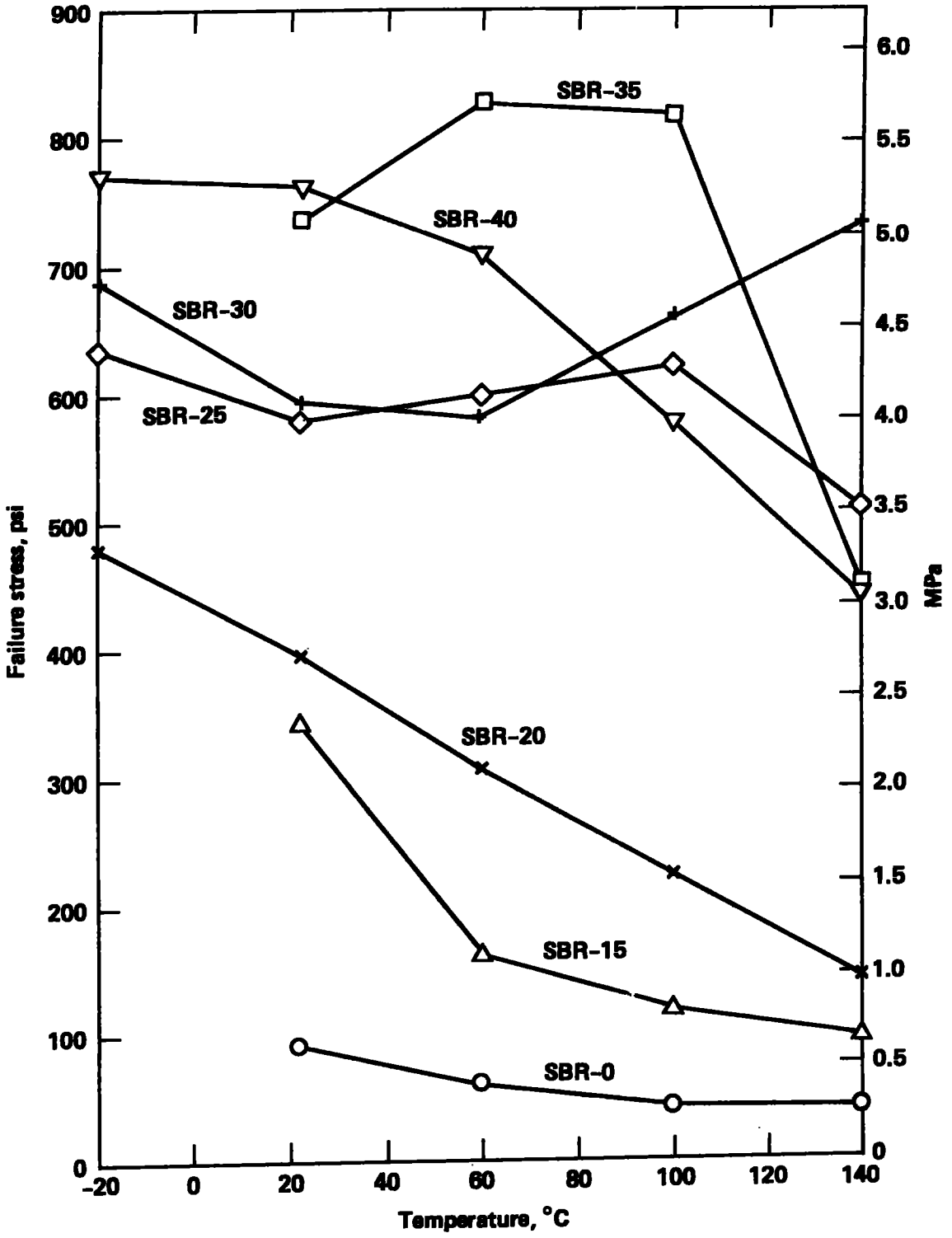


Fig. 19. Failure stress of nicked SBR strip samples tested at various temperatures at a crosshead rate of 0.33 in./s ($\dot{\varepsilon} \approx 10^{-1}$/s).

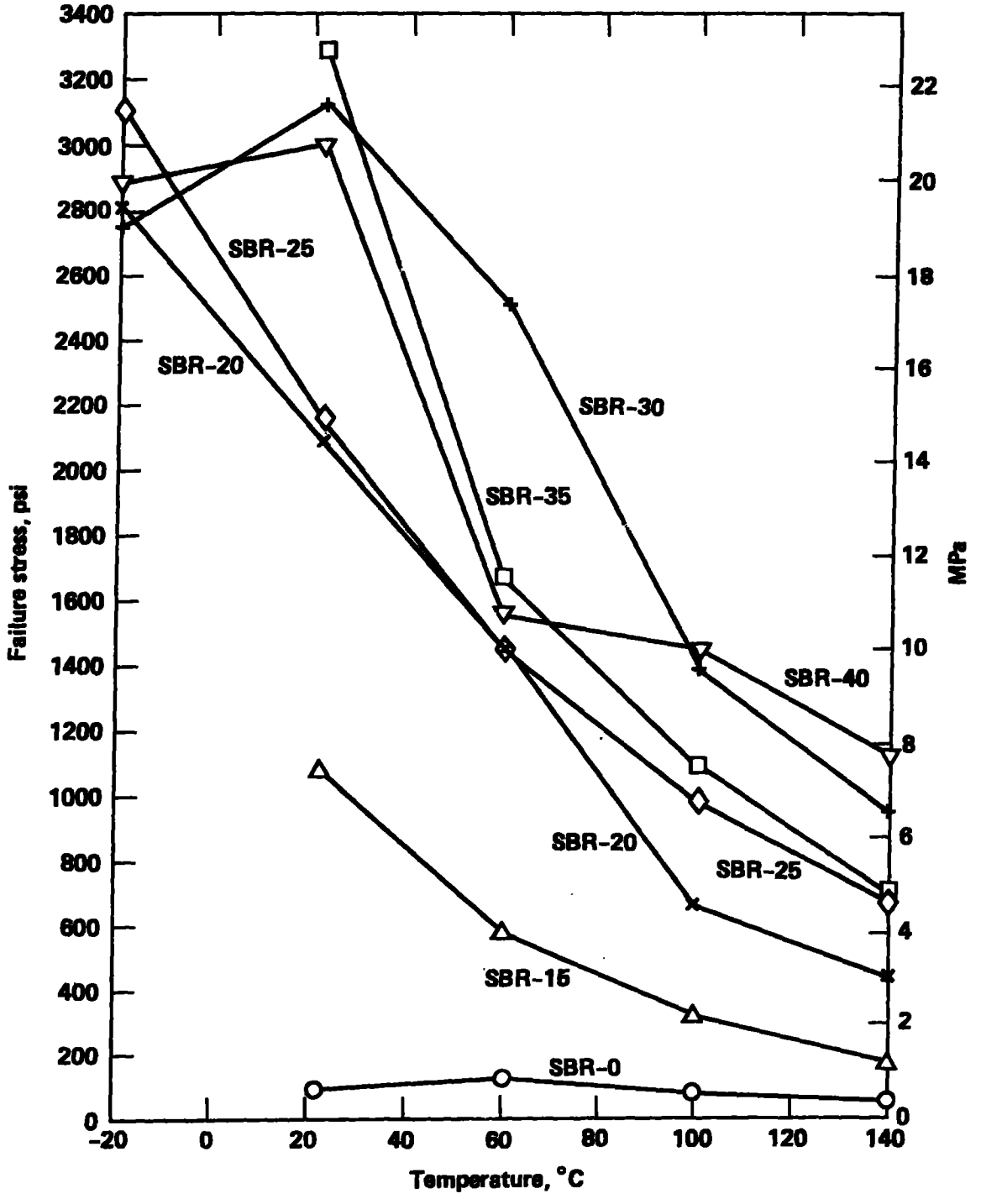


Fig. 20. Failure stress of un-nicked SBR strip samples tested at various temperatures at a crosshead rate of 0.33 in./s ($\dot{\varepsilon} \approx 10^{-1}$/s).

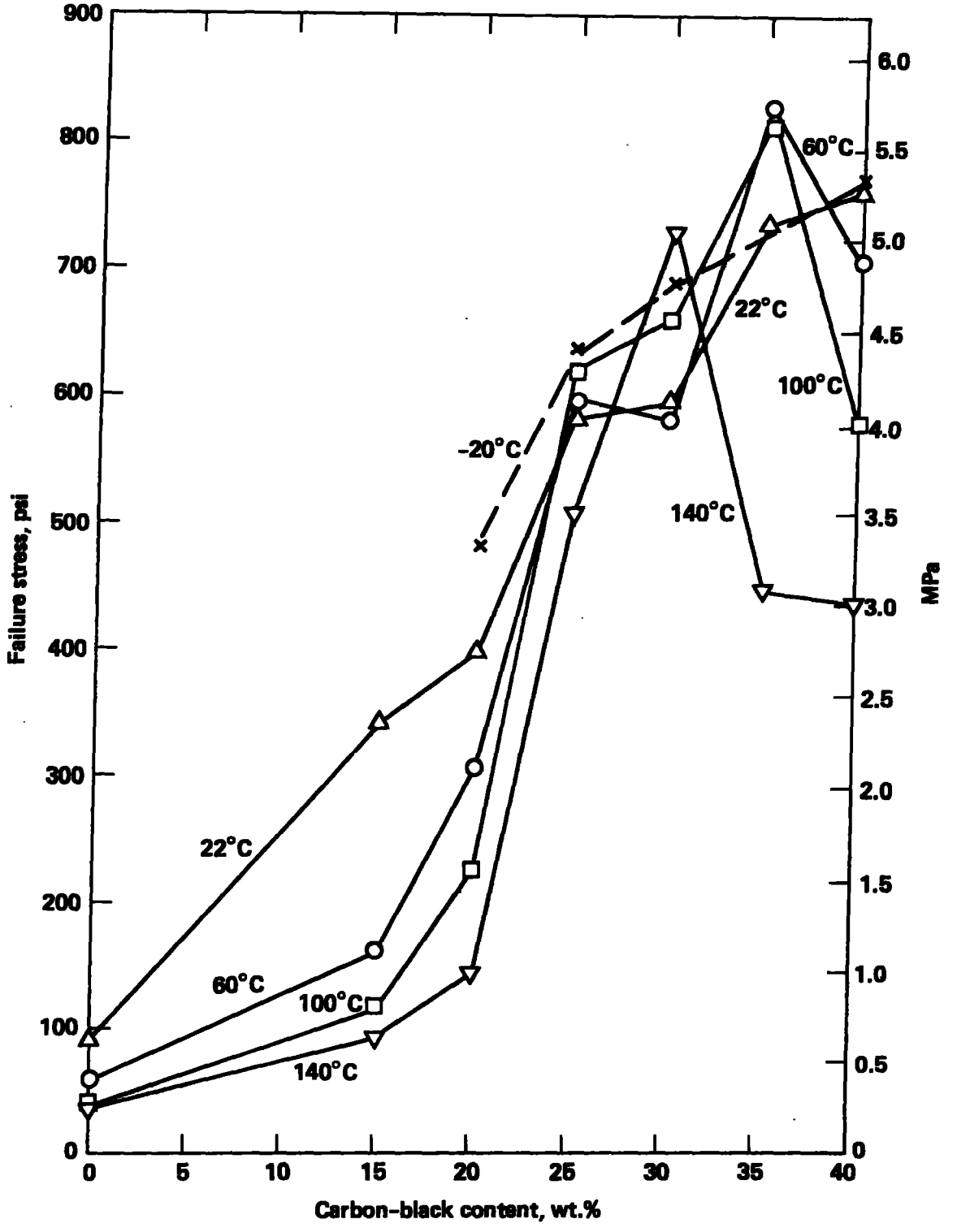


Fig. 21. Failure stress of nicked SBR strip samples as a function of carbon-black content at a series of temperatures. Tested at a crosshead rate of 0.33 in./s ($\dot{\varepsilon} \approx 10^{-1}$/s).

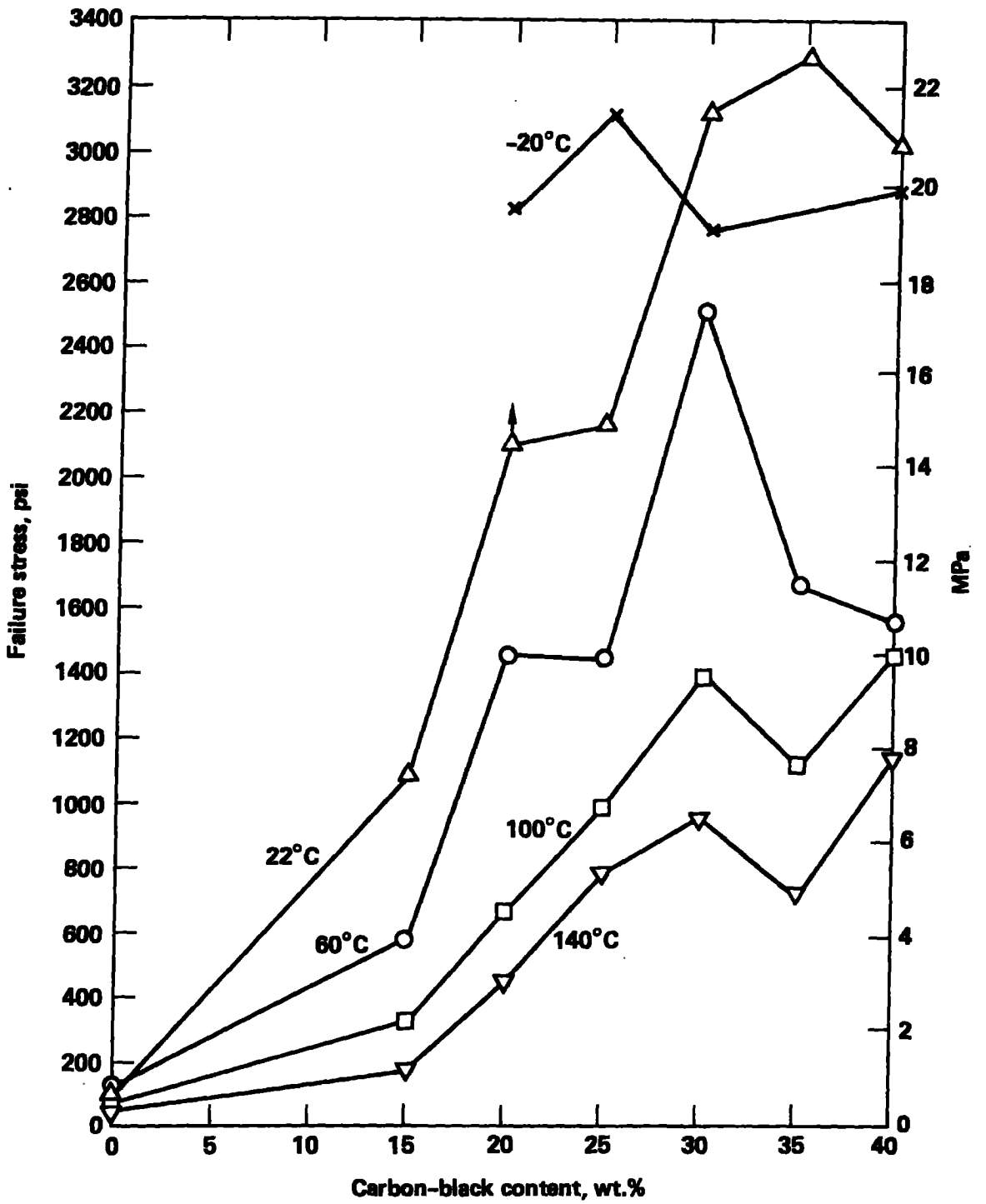


Fig. 22. Failure stress of un-nicked SBR strip samples as a function of carbon-black content at a series of temperatures. Tested at a crosshead rate of 0.33 in./s ($\dot{\varepsilon} \approx 10^{-1}$/s).

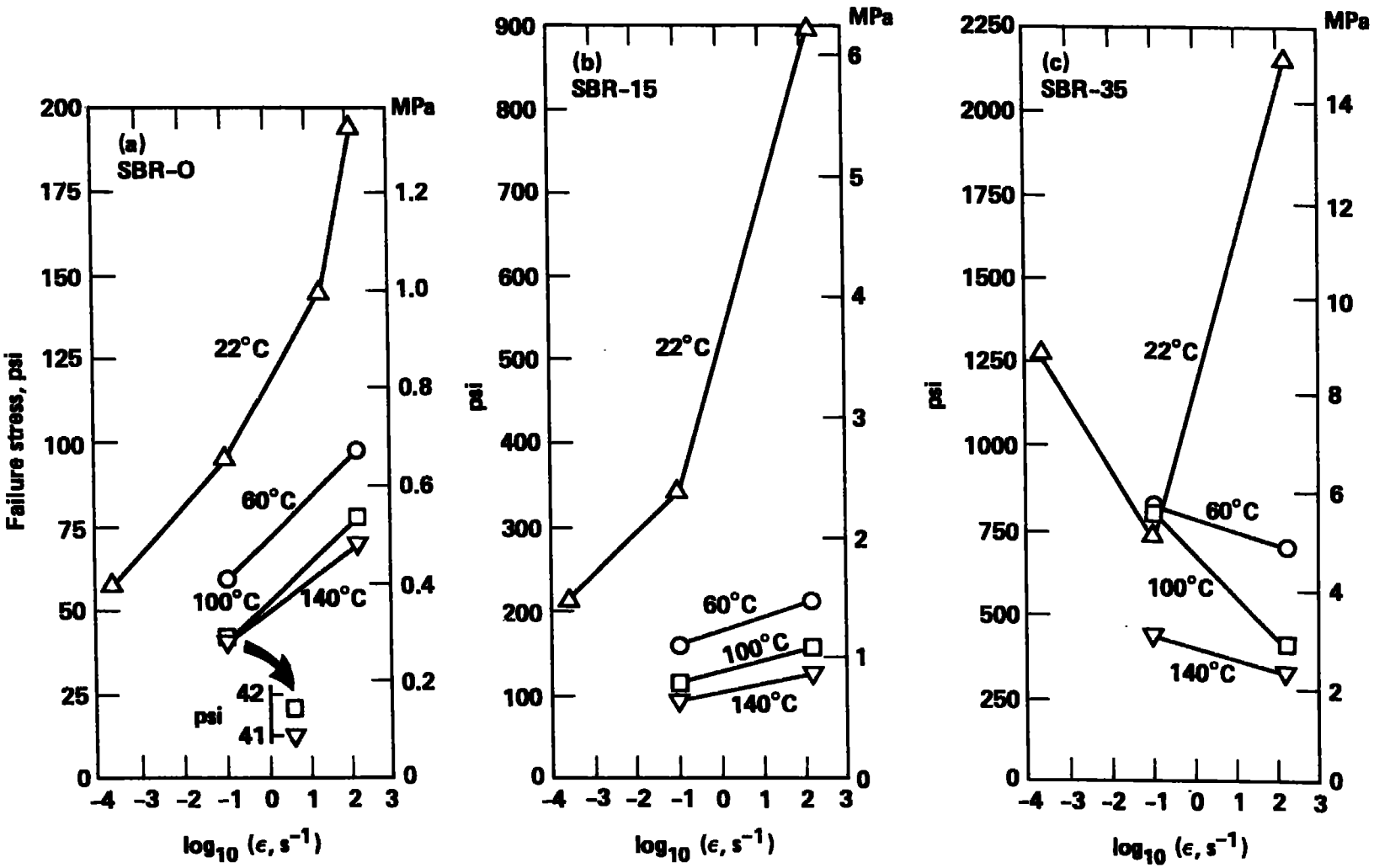


Fig. 23. Effect of strain rate on failure stress at various temperatures for nicked strip samples of SBR-0, -15, and -35.

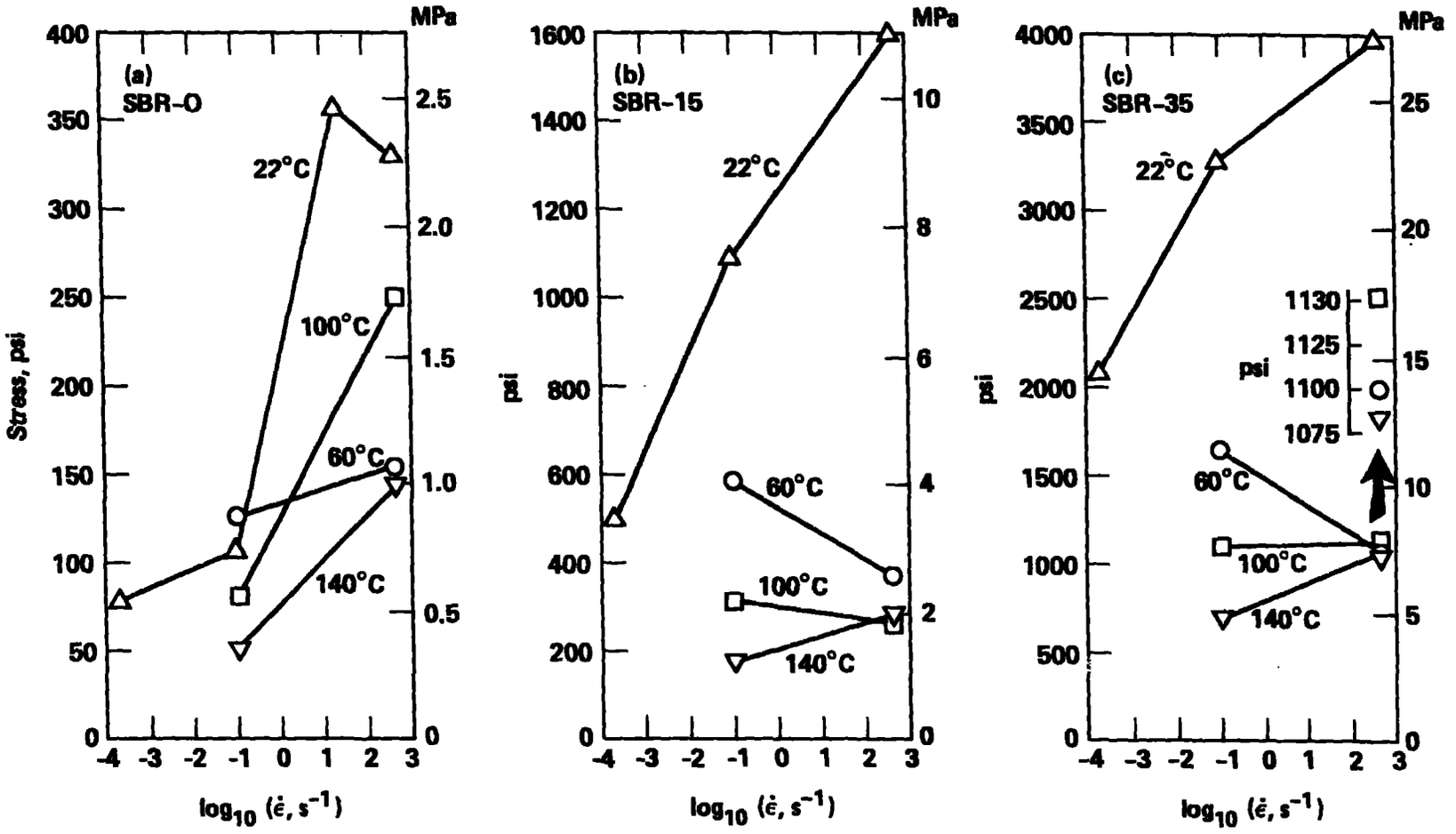


Fig. 24. Effect of strain rate on failure stress or maximum recorded stress at various temperatures for un-nicked strip samples of SBR-0, -15, and -35. NOTE: A number of the SBR-15 and SBR-35 samples could not be taken to failure at the high strain rate.

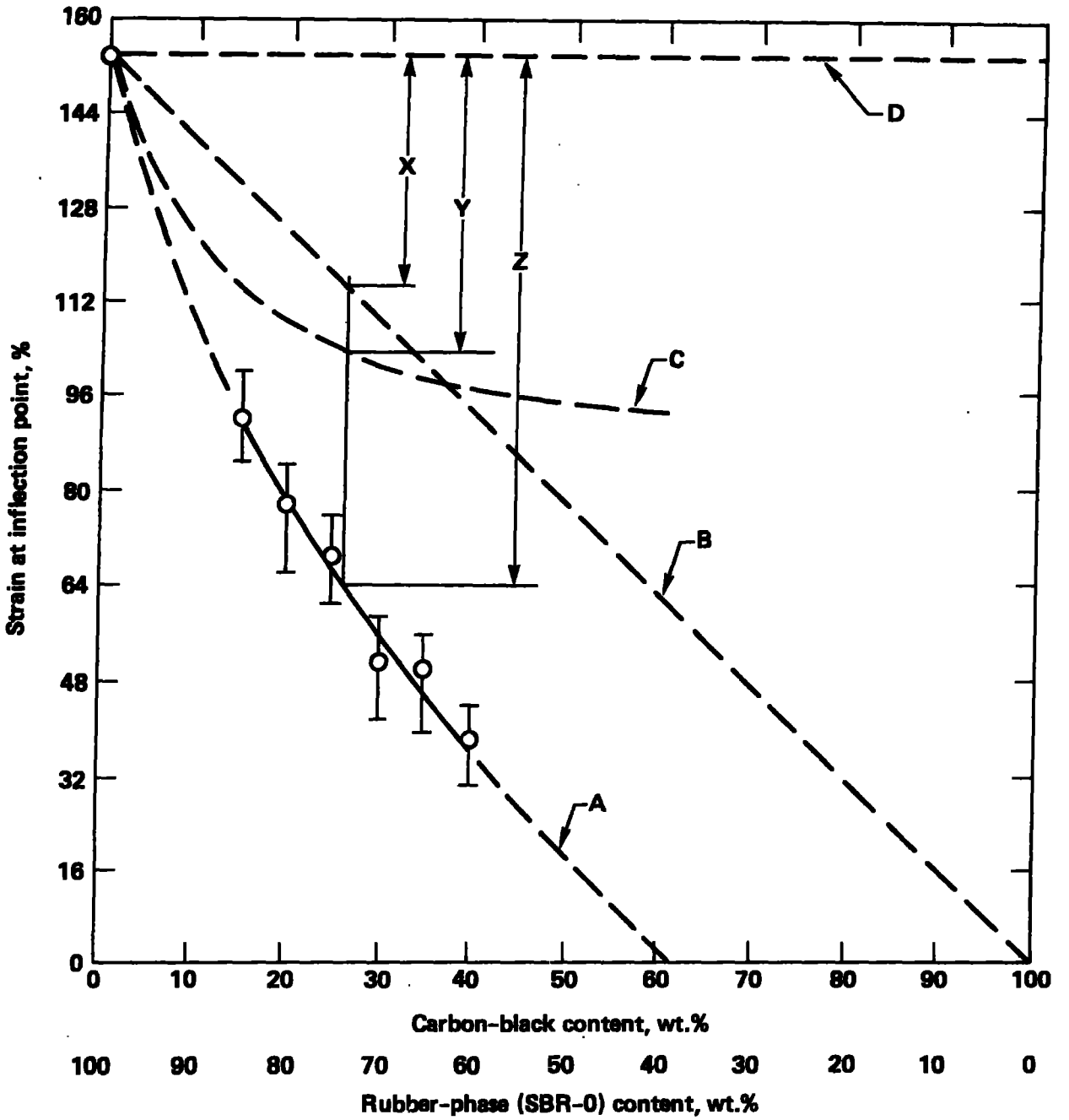


Fig. 25. Effect of filler content on tensile strain at inflection point along the engineering stress-strain curves obtained at a crosshead rate of 0.33 in./s over the temperature range of -20 to 140° C. Curve A refers to experimental data with points representing average values and bars the spread in values; Curve B refers to the effect of rubber phase dilution; Curve C refers to filler-rubber interactions; Curve D refers to a minimum observed inflection strain for SBR-0; Z = X + Y.